REPORT DOCUMENTATION PAGE

Form Approved OMB No. 0704-0188

1. AGENCY USE ONLY (Leave blank)	2. REPORT DATE October 2000	3. REPORT TYPE AND DATES COVERED Final Report

4. TITLE AND SUBTITLE

Characterization Of Semi-Insulating InP Wafers by Scanning Luminescence (SPL), Scanning Photocurrent (SPC) and Cathodoluminescence (CL). Study of the Wafer Homogeneity

5. FUNDING NUMBERS

F61775-99-WE089

6. AUTHOR(S)

Dr. Juan Jimenez Lopez

7. PERFORMING ORGANIZATION NAME(S) AND ADDRESS(ES)

Universidad of Valladolid
ETS Ingenieros Industriales
Valladolid 47011
Spain

8. PERFORMING ORGANIZATION REPORT NUMBER

N/A

9. SPONSORING/MONITORING AGENCY NAME(S) AND ADDRESS(ES)

EOARD
PSC 802 BOX 14
FPO 09499-0200

10. SPONSORING/MONITORING AGENCY REPORT NUMBER

SPC 99-4089

11. SUPPLEMENTARY NOTES

12a. DISTRIBUTION/AVAILABILITY STATEMENT

Approved for public release; distribution is unlimited.

12b. DISTRIBUTION CODE

A

13. ABSTRACT (Maximum 200 words)

This report results from a contract tasking Universidad of Valladolid as follows: The contractor will investigate the distribution of iron in InP wafers using the techniques of scanning photoluminescence and scanning photocurrent.

14. SUBJECT TERMS

EOARD, Semiconductor materials, Indium phosphide

15. NUMBER OF PAGES

79

16. PRICE CODE

N/A

17. SECURITY CLASSIFICATION OF REPORT	18. SECURITY CLASSIFICATION OF THIS PAGE	19. SECURITY CLASSIFICATION OF ABSTRACT	20. LIMITATION OF ABSTRACT
UNCLASSIFIED	UNCLASSIFIED	UNCLASSIFIED	UL

NSN 7540-01-280-5500

Standard Form 298 (Rev. 2-89)
Prescribed by ANSI Std. 239-18
298-102

EOARD Contract SPC 99-4089

Contract order number F61775-99-WE089

Final Report
(October 2000)

CHARACTERIZATION OF SEMIINSULATING InP

WAFERS BY SCANNING LUMINESCENCE (SPL),

SCANNING PHOTOCURRENT (SPC) AND

CATHODOLUMINESCENCE (CL). STUDY OF THE

WAFER HOMOGENEITY

by

J.Jiménez, E.de la Puente, M.Avella, M.A. González

Dpt. Física de la Materia Condensada

Escuela Técnica Superior de Ingenieros Industriales

47011 Valladolid, Spain

UNIVERSIDAD DE VALLADOLID

INTRODUCTION

High quality semiinsulating InP wafers are basic for future developments of advanced optoelectronic and high speed microelectronic devices. Technological improvements of growth and postgrowth processes are necessary if InP has to share the market with other substrates, which the technology is nowadays in a more mature state.

Seminsulating InP is produced by iron doping. The attempts to obtain undoped semiinsulating crystals were not successful and it was concluded that iron must be present in concentration enough to ensure the high resistivity of the substrate. It follows that the engineering of Fe doping is a step forward to the obtention of high quality semiinsulating InP substrates.

Iron doping presents several challenges for the crystal manufacturers, which have to be solved for a healthy future of InP substrates:

    i.   its very small distribution coefficient gives large axial concentration gradients.

    ii.   Only 30-70% of the total iron is electrically active. This means that iron amounts well above the strictly necessary to compensate the residual shallow donors are required

    iii.   The low solubility of iron produces microprecipitates

    iv.   Radial inhomogeneities are observed: e.g. doping growth striations

    v.   Local inhomogeneities: decorated dislocations, faceting...

    vi.   Outdiffusion of iron leads to the contamination of epitaxial layers and the devices based on Fe-doped substrates. The presence of iron in the active part of the devices is detrimental for their performance, since iron is the main carrier lifetime killer in InP.

These points basically contain the main problems related to the presence of iron in InP. Since iron is necessary to obtain semiinsulating InP, the main challenges to obtain high quality semiinsulating InP are:

1. A significant reduction of the iron content, without a concomitant loss of resistivity. This requires to purify the raw materials in order to reduce as much as possible the residual shallow donor concentration.

2. Electrical activation of iron.

3. Improvement of the homogeneity, both at a mesoscopic and a microscopice ranges.

2

4. Additional problems related to the high brittleness of InP have also to be considered, especially for large diameter wafers.
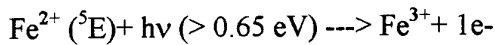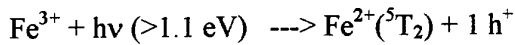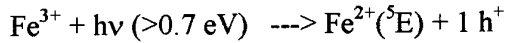
Thermal treatments appear nowadays as the main processes to improve the quality of the InP substrates. The benefit of thermal treatments has been demonstrated in different types of substrates. In the case of InP, and more in particular semiinsulating InP, different annealing approaches have been tried. The annealing parameters have to be optimized in order to obtain noteworthy improvements of the substrate quality in the terms above described.

Commercial InP crystals are grown by either LEC (Liquid Encapsulated Zchralski) or VGF(Vertical Gradient Freeze) growth techniques. This work will exclusively deal with LEC material.
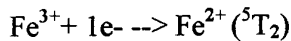
IRON RELATED LEVELS

An excellent review of the main characteristics of iron related levels in InP can be found in the review work done by Bishop [1]. We summarize herein some of the main properties related to the iron electronic levels, which are relevant to the interpretation of our results. In semiinsulating InP electrically active iron is substitutional iron (Fe_{In}); it can be either neutral, Fe^{3+}, or singly ionized, Fe^{2+}, which introduces a mid-gap acceptor level, responsible for the electric compensation of the residual shallow donors. Neutral iron can trap an electron released from a shallow donor converting to Fe^{2+}; while Fe^{2+} can trap a free hole converting to Fe^{3+}. The capture cross sections for electrons ($Fe^{3+}+1e^- ---> Fe^{2+}$) have been reported to range from 1×10^{-15} cm^2 to 4×10^{-14} cm^2 [2-6]. The data for hole capture cross section ($Fe^{2+}+1h^+ ---> Fe^{3+}$), are uncertain and have been estimated to be between 1×10^{-16} and 3×10^{-14} cm^2 [5-7]. Recently, these data have been revised by Söderstrom et al [8] from PL decay measurements in Fe-doped epitaxial layers. They obtained 1×10^{-15} cm^2 for electrons and 6×10^{-15} cm^2 for holes. The intrinsic PL intensity decay was faster when the [Fe2+]/[Fe3+] ratio increased, clearly indicating that $\sigma_p > \sigma_n$. The optical cross sections were measured by Takanoashi et al [9] and fitted to a Lucovsky model [10], Fig.1. The main optical transitions involving iron levels can be summarised as follows: Fe^{3+} is converted to Fe^{2+} when an electron is optically
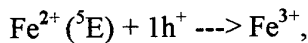
3

excited from the valence band to the Fe^{2+} acceptor level. Fe^{2+} splits out by the crystal field resulting in two electronic levels, the ground state (^5E) and the excited state ($^5T_2$), which are separated each other 0.35 eV. Depending on the excitation wavelength Fe^{3+} can be converted to either the ground (^5E) or the excited ($^5T_2$) state of Fe^{2+}. Electrons are excited from the ground state of Fe^{2+} to the conduction band. These transitions are summarized as follows:
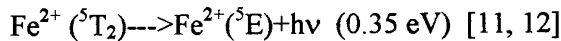
$$Fe^{3+} + h\nu \ (>0.7 \ eV) \ ---> Fe^{2+}(^5E) + 1 \ h^+$$
$$Fe^{3+} + h\nu \ (>1.1 \ eV) \ ---> Fe^{2+}(^5T_2) + 1 \ h^+$$
$$Fe^{2+} \ (^5E) + h\nu \ (> 0.65 \ eV) ---> Fe^{3+} + 1e-$$

The photogenerated electrons recombine at the Fe^{3+} levels:
$$Fe^{3+} + 1e- --> Fe^{2+} \ (^5T_2)$$
while the photogenerated holes recombine at the $Fe^{2+} \ (^5E)$ levels,
$$Fe^{2+} \ (^5E) + 1h^+ ---> Fe^{3+},$$
The excited state of $Fe^{2+} \ (^5T_2)$ decays into the ground state with the emission of 0.35 eV photons:

$$Fe^{2+} \ (^5T_2) ---> Fe^{2+}(^5E) + h\nu \ (0.35 \ eV) \ [11, 12]$$

These transitions constitute the signature of the iron levels in semiinsulating InP, and are used for the assessment of electrically active iron in InP.

WAFER HOMOGENEITY

As a consequence of its very small distribution coefficient the concentration of iron in an ingot present a marked axial gradient, which leads to electrical properties differing from each other wafer of the same ingot.

The lateral homogeneity as well as the homogeneity on a microscale of the electrical properties, are important issues in view of SI InP applications. For instance, the resistivity has been experimentally observed to fluctuate at least 14 % around its mean value along a diameter of commercial SI wafers [13]. The resistivity

4

inhomogeneities are associated with fluctuations of the compensation ratio $\Theta=[Fe_{In}]/[Fe2+]$, defined as the ratio between the total electrically active iron concentration ($[Fe^{3+}]+[Fe^{2+}]$) and the net donor concentration, ($N_D-N_A\approx[Fe2+]$). It is usually recognized that such fluctuations are mainly associated with fluctuations of the iron concentration, since the shallow donors were observed to be distributed quite uniformly [14], in agreement with average segregation coefficients close to one (k=0.8) for common impurities giving shallow donor levels in [15]. This is true on a macroscale but not at a microscopic scale; for instance in the regions surrounding crystal defects their associated strain field can modify the distribution of both iron and donors in relation to the crystal matrix. There are not exhaustive studies about the electrical compensation in the neighbourhood of crystal defects in InP. Only a study on annealed low Fe doped VGF InP was reported combining PL mapping and spreading resistence measurements (16). Both signals were spatially anticorrelated, which was interpreted as a depletion of the iron concentration in the neighborhood of the dislocations. However, there are not similar measurements in as-grown LEC Fe-doped InP. We will discuss later about the electric compensation around crystal defects. We will show that it can be studied combining microPL and microPC measurements. Also DSL (Diluted Sirtl applied with light) etching combined with cathdodluminescence (CL) measurements will provide information about the composition of the surrounding areas.

When the active iron concentration approach the lowest limit of as-grown semiinsulating material ($[Fe_{In}]\approx10^{16}cm^{-3}$) the relative fluctuations of the resistivity across the wafer can reach even 60% of the average value. The resistivity fluctuations in heavily doped material, with compensation ratios > 6, are less sensitive to the changes in the total iron concentration, being less than 10% of the average value along the wafer diameter. This behaviour was observed by D.Wolf et al.[17] studying the resistivity profiles along the diameter of several wafers with different iron concentrations and compensation ratios. They reported resistivity profiles either flat in wafers with high Fe content or very rough in lightly doped material, Fig.2. This fact can be understood by considering the theoretical resistivity vs compensation ratio relations in Fe-doped InP (Fig.3): the fluctuations of the compensation ratio are critical for low compensated material ($\Theta < 3$), in which case a small variation of Θ can give rise to large resistivity changes (in the 60 % range). Although the resistivity variations are not

5

so significant in highly compensated material the iron concentration can present significant fluctuations across the wafer, with regions of high iron concentration, which can have undesirable consequences over other parameters controlled by the iron doping, e.g. the carrier mobility and lifetime, which are critical for the device performances. On the other hand the excess iron is a candidate to outdiffuse and to contaminate the epitaxial layers and the active parts of the devices. It must be also considered that the highest carrier mobilities were measured on samples with low Fe content ($\Theta \approx 2$) [18], therefore, it is clear that a main goal of crystal manufacturers is that of preparing very uniform material with low Fe content and optimal electric properties. The reduction of the iron doping is indeed a step forward towards the improvement of the semiinsulating InP substrates, but such a reduction can only be achieved if there is a concomitant reduction of the residual shallow donor concentration, which can be achieved in two ways, a reduction of the chemical impurities, which can be achieved by a high grade purification of the raw materials, and a reduction of the intrinsic donors in order to ensure the high electrical resistivity. Under such hypotheses, high electrical compensation ratios, homogenous resistivity and good mobility might be obtained.

Regarding the intrinsic donors, hydrogen based complexes have been shown (19, 20) to give a major contribution to the residual donor background. These donors were demonstrated to anneal out, by post-growth thermal treatments. The annihilation of the hydrogen donor complexes was shown to be the main cause for the increase of the resistivity in thermally processed InP..

Since it has been demonstrated that iron is the impurity responsible for the electrical compensation; even in nominally undoped InP converted to semiinsulating by thermal treatment; the assessment of the iron distribution is of high importance for further developments of semiinsulating InP material. The study of the homogeneity is done by means of Scanning Photoluminescence (SPL) and Scanning Photoconductivity (SPC). These techniques allow the obtention of two dimensional maps, which the contrast is correlated to the local composition of the sample. Both PL and PC signals are extremely sensitive to the iron concentration in the two charge states. On the other hand, high spatial resolution can be got by cathodoluminescence. The CL measurements are carried out on specimens selectively etched by the DSL procedure. This etching is very

powerful revealing the atmospheres around crystal defects. The etching rate is governed by the concentration of holes at the solid/liquid interface. This is the reason why the morphology of the revealed atmosphere refflects the impurity distribution around the crystal defects. In this sense, the etching rate is very sensitive to the iron concentration, it reveals growth striations, which are mostly due to the periodic fluctuation of the iron concentration and also the compositional changes surrounding crystal defects.

EXPERIMENTAL SET-UP

Luminescence was measured at room temperature. The excitation was carried out with an argon laser beam (488 nm) focused with a microscope objective, which is also used for the collection of the luminescence emission. The sample is mounted on a high precission motorized XY table. The wavelength of the maximum of the NBG luminescence band was selected in the monochromator and the monochromatic intensity was recorded as a function of the position over the sample. The size of the excitation beam is diffraction limited and the diameter is given by $1.22 \lambda/NA$, where λ is the laser wavelength and NA is the numerical aperture of the objective, this gives an spatial resolution of about 1 μm. The experimental setup is schematically shown in fig.4.

The photoconductivity measurements were carried out at liquid nitrogen temperature in order to enhance the signal to noise ratio due the high dark current at room temperature. The excitation was done with different lines of a cw YAG laser ($\lambda=1.06$ μm or $\lambda=1.32$ μm). The laser beam was focused with a long distance work microscope objective. The sample was mounted on a small cryostat adapted to the motorised XY stage of the microscope. The volume illuminated increases its conductivity by several orders of magnitude, therefore the current measured in the electrometer is due to the illuminated volume. In this case the spatial resolution is not equivalent to that reported for PL measurements. A calculation of the beam path is necessary in order to estimate the volume illuminated by the laser beam. Since PC measurement under excitation with the YAG laser is a volume measurement the results are not dependent on the state of the surface, which is one of the drawbacks of the PL measurements. The sample is translated by means of the motorised stage and scans are

7

done in order to obtain the photocurrent maps. The principle of the method and the experimental set-up are shown in fig.5. For more details see ref. 21-27.

Cathodoluminescence is the luminescence emission excited by an e-beam . It is performed in the SEM (Scanning Electron Microscope) allowing the luminescence imaging with a very high spatial resolution. The CL system is an Oxford monoCL with a liquid nitrogen cooled Germanium detector.

Phase Stepping Microscopy is an interferometry technique used to reproduce the surface topography with nanometer vertical resolution. The system is based in an interferometry microscope objective and high precission piezoelectric displacement element ,oumnted on the microscope objective. The system calculates automatically the topography pf the sample surface from the interferometry fringes obtained at different wave phases

PHOTOLUMINESCENCE AND PHOTOCURRENT LUMINESCENCE CONTRASTS REVISITED

The interpretation of the experimental maps of luminescence and photocurrent requires a previous analysis of the PL and PC signals in relation to the concentration of Fe in order to understand the origin of the contrast in these maps. Models describing the PL and the PC response as a function of the electrically active iron concentration were developed.

In a first approximation the PL intensity can be related to the electrically active iron concentration, the higher the iron concentration, the lower the PL intensity. However, as we have previously mentioned the electrically active iron can be in two charge states, which have different capture cross sections and different concentrations. The same meaning is valid for PC, which is a complex function of the carrier generation rate and the carrier lifetime and mobility. Therefore a meaningful understanding of both the PL and PC signals in Fe-doped InP is necessary in order to understand the PL and PC fluctuations.

8

In the frame of a simplistic model, where the NBG luminescence intensity is inversely proportional to [Fe_{In}] and the extrinsic photocurrent intensity is proportional to [Fe^{3+}], the PC and PL intensities have to be spatially anticorrelated. High [Fe] gives high PC and low PL and viceversa. However, the experience shows that this is not always true and regions with correlated and anticorrelated PC and PL intensities are observed in Fe-doped InP wafers. In the following paragraphs we will set up the rate equations that describe the NBG Luminescence and the extrinsic PC in semiinsulating Fe-doped InP.

According to the electronic transitions previouly described, and the fact that the main non-radiative recombination centers in Fe-doped InP are the iron related levels, we have settled up two rate equation systems accounting for the PC and PL signals respectively. In this sense the monochromatic PL intensity, which is the parameter mapped in our experimental system, must be governed by the ratio between band to band recombination and the capture of free carriers at iron levels.

The rate equations describing the NBG PL are:

$$\frac{dp}{dt} = k\phi - Rpn - C_p p\left[Fe^{2+}\right]$$

$$\frac{dn}{dt} = k\phi - Rpn - C_n n\left[Fe^{3+}\right]$$

$$\frac{d\left[Fe^{3+}\right]}{dt} = C_p p\left[Fe^{2+}\right] - C_n n\left[Fe^{3+}\right]$$

$$\frac{d\left[Fe^{2+}\right]}{dt} = -C_p p\left[Fe^{2+}\right] + C_n n\left[Fe^{3+}\right]$$

$$I_{PL} \propto p_s n_s$$

$$C_p = 10^{-10}; \quad C_n = 10^{-9}; \quad k = 1; \quad R = 10^{-7}; \quad \phi = 10^{20};$$

Where, n and p are the free electron and hole concentrations respectively, n_s and p_s are the corresponding saturation values, Φ is the photon flux, K is the quantum efficiency of the excitation, R is the radiative recombination rate, C_n and C_p are the capture coefficients of iron levels for electrons and holes respectively.

9

A main point for the solution of these equations is the value of the band to band recombination rate, R, in relation to the recombination rates at iron levels, since they are in competition. The capture coefficients by Fe levels are obtained from the litterature (ref.8), the band to band recombination rate is obtained from the article by Klein et al. (28). The characteristic recombination time for e-h pairs is estimated to be 2-3 orders of magnitude smaller than the capture time of electrons by Fe^{3+}. This estimation was further confirmed from the luminescence intensity fluctuations measured in adjacent growth striations assuming a relative iron concentration variation of 20% between adjacent striations, which is a realistic assumption in commercial Fe-doped InP wafers. Growth striations in Fe-doped InP are related to the fluctuations of the iron doping concentration. This suggests that the striations observed by PL mappingnot only obey the fluctuation of the iron concentration, but also the fluctuation of $[Fe^{3+}]/[Fe^{2+}]$ from each other striation.

These equations were numerically solved for different initial $[Fe^{3+}]$ and $[Fe^{2+}]$ concentrations. The results are summarized in fig.6. The luminescence intensity decreases monotonically with the electrically active iron concentration, $[Fe_{In}]$. On the other hand, the decrease is more important when the compensation ratio decreases, showing the influence that $[Fe^{2+}]$ has on the NBG luminescence intensity. Therefore, the luminescence fluctuations are not only due to changes of $[Fe_{In}]$, but also are influenced by the changes of the compensation ratio.

Similar calculations were carried out for the photocurrent. The rate equations in this case are:

$$\frac{dp}{dt} = \sigma_p^0 \phi [Fe^{3+}] - C_p p [Fe^{2+}]$$

$$\frac{dn}{dt} = \sigma_n^0 \phi [Fe^{2+}] - C_n n [Fe^{3+}]$$

$$\frac{d[Fe^{3+}]}{dt} = -\sigma_p^0 \phi [Fe^{3+}] + \sigma_n^0 \phi [Fe^{2+}] + C_p p [Fe^{2+}] - C_n n [Fe^{3+}]$$

$$\frac{d[Fe^{2+}]}{dt} = \sigma_p^0 \phi [Fe^{3+}] - \sigma_n^0 \phi [Fe^{2+}] - C_p p [Fe^{2+}] + C_n n [Fe^{3+}]$$

$$I_{PC} = \mu_p e S E \left(\frac{\mu_n}{\mu_p} n_s + p_s \right)$$

$$\sigma_p^0 = 3{,}69 * 10^{-17}; \quad \sigma_n^0 = 2{,}11 * 10^{-18}; \quad \phi = 10^{20};$$

$$C_p = 10^{-10}; \quad C_n = 10^{-9}; \quad \mu_p = 10^3; \quad S = 2 * 10^{-7} cm^2;$$

$$E = 100 \frac{V}{cm}; \quad \frac{\mu_n}{\mu_p} = 10$$

$$I_{PC} = 3{,}2 * 10^{-21} (10 n_s + p_s)$$

σ_p^0 and σ_n^0 are the hole and electron optical cross sections. E the electric field, μ_n and μ_p the electron and hole mobilities, S the section of the illuminated volume.

The solution for the same iron concentrations used to obtain the results of fig.6 are shown in Fig. 7. In this case the photocurrent increases when the iron concentration increases and for equal total iron concentration it increases when $[Fe^{3+}]$ increases. In other words, the PC intensity is mostly determined by the compensation ratio, the higher the compensation ratio, the higher the photocurrent intensity. Note that in our experimental set-up the measured photocurrent intensity is the saturation intensity, since the scanning system is much slower than the characteristic response time of the photocurrent.

Using these results we have traced plots where we represent $[Fe^{2+}]$ vs $[Fe^{3+}]$ over which the luminescence and the photocurrent remain constant, fig. 8. The signs + and -

11

indicate respectively the sense of increase and decrease of either PL or PC. Therefore the regions inside the crosses with the same sign for PL and PC represent correlation, while the regions with different sign represent anticorrelation.

These plots are very useful for the interpretation of the PL and PC maps. The first consequence extracted is the possibility of either correlation and anticorrelation between PL and PC signals depending on the local concentrations of iron and residual donors. Note that the regions indicated by a and c correspond to anticorrelation and correlation respectively. Roughly, one can estimate that spatial correlations should be controlled by the variations of the residual donor concentration ($[Fe^{2+}]$), while the spatial anticorrelations are dominated by the variations of the electrically active iron concentration $[Fe_{In}]$, or the neutral iron population, $[Fe^{3+}]$.

We have already mentioned that the photocurrent intensity is mainly determined by the compensation ratio. If one represents in the plot of Fig.8 lines of constant compensation, they are very close to the lines of constant photocurrent. They slightly deviate from those lines for the high compensation ratios.

ANALYTICAL SOLUTIONS

Now, we will search for analytic expressions that could account for the calculated results and would provide a simple interpretation of the experimental results.

Assuming that the iron concentrations under illumination are mainly modified by the generation and the capture of holes, one can obtain the following expression for the free hole concentration in steady state conditions:

$$p_s = \frac{-\left([Fe^{2+}]_i + \frac{\sigma_p^0 \phi}{c_p}\right) + \sqrt{\left([Fe^{2+}]_i + \frac{\sigma_p^0 \phi}{c_p}\right)^2 + 4 \frac{\sigma_p^0 \phi}{c_p}[Fe^{3+}]_i}}{2} \qquad [3]$$

The electron concentration can be approximated by:

12

$$n_s = \frac{\sigma_n^0 \Phi([Fe^{2+}]_i)}{C_n[Fe^{3+}]} \qquad [4]$$

This concentration is significantly lower than the concentration of holes; it only becomes relevant for low compensation ratios (< 3).

Therefore the PC intensity can be written as:

$$I_{PC} = 3.2 * 10^{-21}\left(10\,\frac{\sigma_n^0 \phi [Fe^{2+}]_i}{C_n[Fe^{3+}]_i} + \frac{\sqrt{\left([Fe^{2+}]_i + \frac{\sigma_p^0 \phi}{C_p}\right)^2 + 4\frac{\sigma_p^0 \phi}{C_p}[Fe^{3+}]_i}}{2} - \frac{[Fe^{2+}]_i + \frac{\sigma_p^0 \phi}{C_p}}{2} \right)$$

$$[5]$$

This expression can be expressed in a more compact form as follows:

$$z_5 = 6.75 * 10^{-9}\,\frac{z_{4i}}{z_{3i}} - 1.6 * 10^{-5}\left(z_{4i} + 3.69 * 10^{-3}\right) + 1.6 * 10^{-5}\sqrt{\left(z_{4i} + 3.69 * 10^{-3}\right)^2 + 1.48 * 10^{-2} z_{3i}}$$

$$[6]$$

where, z_3, z_4, z_5 are:

$$z_3 = \frac{[Fe^{3+}]}{10^{16}}; \quad z_4 = \frac{[Fe^{2+}]}{10^{16}}; \quad z_5 = I_{PC}.$$

The subindex i refers to the initial values.

Developing the square root of eq. as a Taylor's series in powers of $z_3/z_4 = [Fe^{3+}]/[Fe^{2+}]$ it is possible to approximate the PC intensity by an expression in which the compensation ratio appears explicitly:

$$(z_5)_{PC} = \frac{6.75 * 10^{-9}}{\left(\dfrac{z_{31}}{z_{4i}}\right)} + 1.6 * 10^{-5}\left[0.72 * 10^{-2}\frac{z_{31}}{z_{4i}} - 0.27 * 10^{-4}\left(\frac{z_{31}}{z_{4i}}\right)^2 \frac{1}{z_{4i}} + \ldots\ldots\right] \quad [7]$$

The dominant term is the first one in the brackets. This linear relation is reasonably valid for compensation ratios below 10, which is the typical compensation ratio of commercial semiinsulating InP wafers. This analytical expression reproduces with high accuracy the results obtained numerically when solving the photocurrent rate equations. The error introduced in this approximation as compared to the calculated PC intensity is less than 1% over the range of concentrations considered, which lie inside the limits of commercially avilable Fe-doped InP wafers.

A similar approach can be done for the photoluminescence intensity. First, we can assume that $[Fe^{3+}]$ and $[Fe^{2+}]$ do not change significantly by electron and hole captures. This approach is reasonable for a band to band recombination rate significantly higher than the capture rates by Fe^{2+} and Fe^{3+} repectively.

Under this assumption one obtains the following expression for the NBG photoluminescence intensity:

$$I_{PL} = p_s n_s = \frac{2k\phi R + C_p C_n [Fe^{3+}]_i [Fe^{2+}]_i - \sqrt{(C_p C_n [Fe^{3+}]_i [Fe^{2+}]_i)^2 + 4k\phi R C_p C_n [Fe^{3+}]_i [Fe^{2+}]_i}}{2R^2}$$

$$[8]$$

Therefore the PL intensity fluctuations are associated with the fluctuations of the product $[Fe^{3+}]*[Fe^{2+}]$; in fact the PL intensity decreases when this product increases and viceversa.

The accuracy of this expression is improved when one corrects $[Fe^{3+}]$ and $[Fe^{2+}]$ taking into account the changes introduced under illumination, then the analytical expression obtained is:

14

$$z_5 = 10^{-4} + 5 * 10^{-4}(P + \Delta P) - 5 * 10^{-4}\sqrt{(P + \Delta P)^2 + 0,4(P + \Delta P)}$$

$$P = z_{3i}z_{4i}$$

$$\Delta P = \left(-5 * 10^{-4}P + 5 * 10^{-4}\sqrt{P^2 + 0,4P}\right)\left(10^2 z_{3i} - 10z_{4i}\right)\frac{z_{3i} - z_{4i}}{z_{3i}z_{4i}}$$

with

$$z_1 = \frac{p}{10^{16}}; \quad z_2 = \frac{n}{10^{16}}; \quad z_3 = \frac{\left[Fe^{3+}\right]}{10^{16}}; \quad z_4 = \frac{\left[Fe^{2+}\right]}{10^{16}}; \quad z_5 = z_1 z_2$$

or in terms of the iron concentrations:

$$\Delta P = \frac{-C_p C_n P + \sqrt{\left(C_p C_n P\right)^2 + 4k\phi RC_p C_n P}}{2RC_p C_n P}\left(C_n\left[Fe^{3+}\right]_i - C_p\left[Fe^{2+}\right]_i\right)\left(\left[Fe^{3+}\right]_i - \left[Fe^{2+}\right]_i\right)$$

[9]

the subindex i refers to the initial concentrations.

Using this expression the agreement with the PL calculated solving the rate equations is better than 1%. If we make a look to the analytical solutions we can deduce that the photocurrent intensity is proportional to the $[Fe^{3+}]/[Fe^{2+}]$ ratio, while the PL intensity decreases when the product $[Fe^{3+}]*[Fe^{2+}]$ increases. The plots of Figs. 9 and 10 correspond to the relation between the concentrations of the two charge states of the electrically active iron $[Fe^{3+}]$ and $[Fe^{2+}]$ for constant values of the PC and PL intensities calculated from the numerical solution of the rate equations, the analytical solution according to equations 5 and 8, and the constant $[Fe^{3+}]*[Fe^{2+}]$ and $[Fe^{3+}]/[Fe^{2+}]$ amounts. The excellent agreement between the three plots allows a simple interpretation of the PL and PC fluctuations in terms of the $[Fe^{3+}]$ and $[Fe^{2+}]$ concentrations.

In summary, the PC intensity is mostly determined by the $[Fe^{3+}]/[Fe^{2+}]$ ratio, while the luminescence intensity decreses when the $[Fe^{3+}]*[Fe^{2+}]$ increases. Depending

on the local compensation one can observe spatial anticorrelation or spatial correlation between both signals.

PHOTOLUMINESCENCE AND PHOTOCURRENT RESULTS

As-grown wafers

PC and PL maps were obtained in as-grown Fe-doped InP wafers. Some characteristic maps are sown in figs 11-12. The main experimental features of the PL maps in as-grown Fe-doped InP are:

i.- The existence of concentric rings of high and low PL intensity, fig.11. The radii of adjacent rings differ a few μm each other. This pattern is due to the doping growth striations.

ii.- The existence of dispersed bright spots, which correspond to small structures (micrometric size) with high PL emission, fig.12.

iii.- The existence of some big structures (from hundreds micrometers to a few mm's) with differentiated PL emission, fig.11.

iv.- In general the luminescence intensity decreases from the center to the rim of the wafer. The fluctuations are organised as concentric rings with the center in the crystal axis. Contrarilly to the structure reported in i) the period between the different rings is in the mm's-cm's scale, in fact, the growth striations appear supperposed to the long range background intensity.

i) ii) and iv) are general features of the as-grown Fe-doped InP wafers, while iii) is not a general observation, it is probably the cause of some growth incident. It looks as a big inclusion. In support of this hypothesis one can note the full absence of the growth striations inside this region, the o-ring pattern typical of the growth striations is sharply interrupted at the borders of this structure. On the other hand, the lower luminescence

16

intensity suggests a higher iron concentration inside the volume occupied by the inclusion. The sharp change in the luminescence intensity at the border of the inclusion suggests the presence of low angle grain boundaries.

The long range PL distribution and the concentric rings, are associated with the iron distribution at macroscopic and mesoscopic scales. According to the interpretation of the PL contrast discussed in the previous section the fluctuations of the PL intensity are determined by the product $[Fe^{3+}]*[Fe^{2+}]$, when this product increases the PL intensity decreases. The $[Fe^{3+}]*[Fe^{2+}]$ product can increase because one of the factors increases its value, remaining the other one nearly constant, or because the two factors approach each other leaving the sum nearly constant. The two possibilities have different meanings, the first one corresponds to the fluctuation of the iron concentration with a nearly unchanged residual donor distribution, while the other possibility suggests a more important contribution of the shallow donor fluctuations. According to the distribution coefficient of iron in InP, we have to consider more reliable the first hypothesis, in fact a true distribution of the electrically active iron concentration, $[Fe_{In}] = [Fe^{3+}]+[Fe^{2+}]$, must exist. This should mean that the main variation of the luminescence intensity is due to the fluctuations in $[Fe^{3+}]$. This interpretation agrees with the high segregation coefficient of the residual donors ($\cong 0.8$).

The microscopic fluctuations of the luminescence intensity present dispersed bright spots. Since the luminescence intensity is decreased when the $[Fe^{3+}]*[Fe^{2+}]$ product increases one can assume that the local enhancement of the luminescence intensity is due to either a decrease of the Fe concentration or a decrease of the shallow donor concentration. These bright spots have been associated with the atmospheres of the dislocations, and the region surrounding the iron microprecipitates. This can result from the gettering action of the dislocations, which leave the surrounding areas free of iron. Also the gettering of the residual donors has similar results in the luminescence intensity since it lowers the $[Fe^{2+}]$ concentration. Both mechanisms lead to a decrease of the $[Fe^{3+}]*[Fe^{2+}]$ product with the corresponding enhancement of the luminescence intensity.

17

We present in fig.13 a detailed image of the photoluminescence distribution in one of those bright spots and the luminescence intensity profile. The luminescence pattern suggests that it is associated with a grown-in dislocation. It consists of a central dark spot surrounded by a bright halo. The dark central point is due to the non radiative recombination at the dislocation core. The surrounding area is the defect depleted region due to the gettering action of the dislocation. This luminescence pattern is typical of iron doped InP. It could be due to the gettering of iron at the dislocation, however, it might be possible that gettering of residual donors could contribute to the observed luminescence distribution. The luminescence intensity in the Cottrell atmosphere is enhanced by a factor 3 compared to the matrix. In standard commercial wafers this fluctuation should correspond to a $[Fe_{In}]$ reduction over one order of magnitude assuming that only iron is responsible for this observation. However, if there is also a concomitant reduction of the residual donor concentration, the total iron concentration decrease necessary to account for the sharp luminescence enhancement should be significantly reduced. In fact the best compromise to account for such a strong photoluminescence contrast is an overall reduction of the iron and residual donor concentrations with an increase of the compensation ratio, see the theoretical plot of Fig.7, where it clearly appears that high luminescence increases are associated with the two effects we have noted here.

DSL ETCHING AND CATHODOLUMINESCENCE

A few crystal defects were studied by DSL and Cathodoluminescence imaging in order to study the nature of the atmospheres surrounding these defects. The crystal defects were revealed by DSL etching. The typical objects revealed are grown-in dislocations, clusters of grown in dislocations or precipitates, inclusions... . After revealing crystal defects by DSL, measurements of PSM (Phase Stepping Microscopy) and cathodoluminescence were carried out. PSM is an interferometry technique allowing surface topography with nanometer vertical resolution, which allows a characterization of the etching rate around the crystal defects. DSL is a selective etching, which the etching rate is proportional to the free hole concentration at the solid /liquid interface. The etching rate is reduced in the absence of such holes, which in the DSL procedure are photogenerated by a halogen lamp or supplied by the acceptor

levels. The main source of holes for such broad spectral distribution light are iron levels. This is supported by the PC maps obtained with either monochromatic (1.06 μm) or white (halogen lamp) lights, the photocurrent distribution is nearly the same for both excitation sources, Fig.14, which suggests that the main source of free carriers and the main recombination centers in both cases are the same; taking into account the analysis of the photocurrent excited with 1.06 μm light one can conclude that the iron levels are also the main source of free holes when the excitation is achieved with white light from a halogen lamp. Therefore, a reduced concentration of iron would result in a reduced etching rate, because of the lower photo-generation rate of holes. Another hypothesis for slow etching rate is a large concentration of iron, which slows down the the etching rate because of the active hole recombination rate at iron levels.

Cathodoluminescence images, PSM topographies and step profiles of some of the revealed defects are shown in figs 15-18. The first observation is that most of the revealed structures appear as hillocks, which means that the etching rate is smaller in relation to the etching rate at the surrounding matrix. This should be correlated to brihgter luminescence emission of the defect areas as observed in the CL images, which suggests that the overall iron concentration is low in these regions, or according to the discussion of the PL contrast, the $[Fe^{3+}]*[Fe^{2+}]$ is small, which could be explained by a low iron concentration or a reduced $[Fe^{2+}]$. In other words, the low etching rate observed in these structures is mostly due to the low iron and shallow donor concentrations in the areas surrounding the crystal defects. The low iron concentration will be responsible for the low photogeneration of holes, especially when $[Fe^{2+}]$

PHOTOCURRENT MEASUREMENTS

A typical photocurrent map of an as-grown Fe-doped InP wafer is represented in fig.14. A typical fourfold symmetry is observed. Since the photocurrent intensity is proportional to the $[Fe^{3+}]/[Fe^{2+}]$ ratio, one can assume that the photocurrent pattern roughly reproduces the resistivity distribution across the wafers. Such a pattern is also typical of the stress distribution of as-grown wafers by the LEC method.

19

The fourfold symmetry distribution of the PC maps suggests that the $[Fe^{3+}]/[Fe^{2+}]$ ratio is correlated to the dislocation pattern, which exhibits the typical fourfold pattern in LEC crystals. Some big structures are observed, which are characterized by an intense photocurrent, they are observed for all the wafers studied, which were consecutive wafers of the same ingot. The PC pattern associated with this structure presents an elongated form starting at the crystal edge. These large crystal defects can be related to twining or polycrystallinity, which are typical crystal structure breakdowns in LEC <001> InP. Iron seems to accumulate in this region, as deduced from the very high PC intensity associated with this structure. These structures give low PL intensity, which suggests the accumulation of iron in these regions, though it does not appear so well resolved in PL maps, which suggests that this region is heavily compensated, but the product of both iron concentrations does not change so sharply as the compensation ratio.

The PC maps do not reveal the two dimensional pattern associated with the growth striations. This fact can be explained in two ways: i) the growth striations are not revealed because the $[Fe^{3+}]/[Fe^{2+}]$ ratio remains nearly constant over adjacent growth striations, which suggests equivalent seggregation coefficients for iron and residual donors, however the seggregation coefficient of these species differ each other by almost two orders of magnitude, 0.001 vs 0.8. This hypothesis seems rather improbable in view of the differences expected between the distributions of iron and residual donors. Note that the PC intensity is mostly sensitive to changes in the compensation ratio over the full range of compensation ratios expected in commercial semiinsulating InP. ii) The absence of growth striations in the PC maps is inherent to the PC method itself. Note that the PL emission arises from the top surface of the sample, the laser probes only a few hundred nm's depth; however, PC probes the bulk since the sample is transparent to the excitation light. If we take into account the concavity of the liquid solid interface, we can conclude that the sidewalls of the growth striations are not perpendicular to the wafer plane, but they have a non negligible inclination, which depends among other factors of the pulling rate. Taking into account the typical wafer thickness, ≈ 500 μm, one can deduce that the laser beam is probing simultaneously different growth striations, stratified across the wafer. In order to check this, PL maps were obtained on both the front and the back sides of a wafer. The growth

20

striations were revealed on both sides and then the images were glided along a diagonal to get them into coincidence, fig.19. The gliding distance along the diagonal accounts for the above interpretation of the absence of the growth striation pattern in PC maps; in fact, a laser beam crossing throughout the wafer is probing simultaneously several growth striations, therefore the photocurrent signal is an average of PC signals arising from them. Contrarily to the growth striations pattern the long range inhomogeneity pattern is well reproduced by PC mapping, since the drawbacks related to the sample thickness are not relevant for that type of inhomogeneities.

A typical photocurrent scan of an old specimen is shown in fig. 20. This scan differs from scans obtained on crystals grown with the actual state of the art. In this specimen the PC scan reveals regular sharp photocurrent peaks. This type of signature is not common for the actual commercial wafers for which the photocurrent scans at the lateral scale of fig.20 give a smooth intensity profile. These peaks which appear more or less regular are not growth striations as the two dimensional pattern was not reproduced.

An interesting observation is the fact that the photocurrent appear always as high photocurrent features superposed onto a smooth background. This should mean that the local photocurrent features are always related to increases of the $[Fe^{3+}]/[Fe^{2+}]$ ratio. This does not mean that the iron concentration is locally enhanced, but only that the local compensation ratio has increased in relation to the background, either by an increase of the iron concentration or by a decrease of the shallow donor concentration; note that even a decrease of the iron concentration can produce an increase of the $[Fe^{3+}]/[Fe^{2+}]$ ratio if the shallow donor concentration is decreased an amount higher than the iron decrease.

In this sense, it should be noted that the PL maps do not give usually profound intensity depressions; only some of them appear related to scratches where the non radiative recombination is very efficient. Out of this handling defects the luminescence inhomogeneities appear as bright spots. The scratches are not observed in PC maps, because they are surface defects, while the PC signal arises from the bulk, which reduces substantially the contribution of the short carrier lifetime near the scratch to the photocurrent signal. Therefore, the PL features are very close to that observed by PC

21

and suggests that the origin of the local inhomogeneities observed by both techniques consists of the local concentration decrease of both iron and shallow donors. Note also that this overall reduction of point defects produces an enhancement of the carrier mobility, which gives an additional enhancement to the photocurrent signal.

The microfluctuations of the photocurrent are shown in Fig.21. These inhomogeneities are associated with local fluctuations of the compensation ratio and are rather probably related to crystal defects. Although the shape of these structures revealed by PC mapping is similar to that revealed by PL mapping, a full coincidence between PL and PC microstructures cannot be done by instance.

PL AND PC AROUND CRYSTAL DEFECTS

We have already discussed about this question in previous paragrahs. The crystal defects are centers for point defect gettering under the action of their stress field. From the above discussions we claimed about a reduction of the total iron concentration and shallow donor concentration, being the late more intensely reduced. In tis sense, what we can expect around a crystal defect is an increase of the luminescence intensity and an increase of the photocurrent intensity.

The behaviour of PC and PL signals around crystal defects is interesting in order to understand the distribution of both $[Fe^{3+}]$ and $[Fe^{2+}]$ at a microscopic scale. Some crystal defects were revealed by photoetching. PL and PC maps were obtained on these crystal defects. The PL and PC maps of an extended crystal defect together with the Nomarski micrograph are shown in fig.22. The crystal defect as revealed looks as alow angle grain boundary. Both PL and PC intensities appear correlated. The PL and PC signals are enhanced at the Cottrell atmospheres in agreement with the previous arguments. Taking into account the gettering action of the dislocations, one can assume that the iron concentration is decreased at the Cottrell atmosphere, with the corresponding PL enhancement; however, the fact that the PC intensity is enhanced suggests that also the compensation ratio is increased. Both facts can be reconciled if one assumes that both the iron concentration and the residual donor concentration are reduced at the Cottrell atmosphere. This is consistent with the previous discussion about

22

CL, DSL etching and PC and PL fluctuations. In conclusion, the Cottrell atmospheres are regions of low iron concentration and high electric compensation. This behaviour appears more evident after thermal treatment, when the outdiffusion during the annealing enhances the gettering by the crystal defects. Note that the difference of spatial resolution between PL and PC, could mask some details of the PL and PC correlation around the crystal defects. In Fact, the PL map appears more defined than the PC map, which is expected from the superior spatial resolution of this technique.

THERMAL TREATMENTS

Thermal treatments have been demonstrated to improve the quality of Fe-doped InP (16, 25, 31-39). The aim of the annealing process is to decrease the iron concentration, to get it more uniform and therefore to improve the electrical properties. Different routes can be followed to achieve improvements of the susbtrates.

These methods are summrized as follows:

i.   Annealing of undoped semiconducting InP

ii.   Annealing of lightly Fe doped semiconducting InP.

iii.   Annealing of Fe- doped semiinsulating InP.

iv.   Annealing of semiconducting undoped InP in the presence of an iron source.

Undoped semiconducting InP

Method i has been shown to lead to high resistivity InP; however, the poor reproducibility of the process make it a difficult route to obtain high quality semiinsulating InP substrates. The lack of reproducibility is tightly related to the fact that the electric compensation is due to background residual iron, which becomes

23

enough to ensure electric compensation if the residual shallow donors are outdiffused in concentration enough. In fact, the Hydrogen related complexes, $V_{In}-(PH)_4$ complexes, are assumed to be the shallow donors removed during the annealing process. Therefore, the resultant high resistivity depends on the balance between the residual iron concentration and the residual donor impurities. The success on the obtention of semiinsulating material depends on the purification of the raw materials.

Lightly Fe-doped Semiconducting InP

This method ii is the consequence of the previous discussion. In fact, the semiinsulating behavior cannot be achieved with residual iron concentration below $8-10*10^{14}$ cm^{-3}. Since this depends on the purity of the raw materials an alternative approach is the annealing of the semiconducting material with a preadjusted iron concentration, which must range between 10^{15} and $5*10^{15}$ cm^{-3}. The situation is summarized in Fig.23, where the resistivity vs the iron concentration for undoped annealed InP and as-grown semiinsulating Fe-doped InP is represented

This annealing procedure warrants the obtention of semiinsulating material after adequate thermal treatment. Some results concerning semiinsulating InP samples obtained by this method are presented here. Two semiconducting Fe-doped samples were annealed under the standard optimal conditions determined from annealing experiments of semiinsulating InP. These conditions were: $T_{annealing}>900^oC$, $t_{annealing} >50$ hours and cooling rates between 30 and 60 °C/min and small phosphorous pressure. These annealing conditions warrant effective anneal out of $V_{In}-(PH)_4$ complexes, electrical activation of iron, solving of the precipitates and stability of the surfaces. The conjunction of these processes gives an improvement of the electrical properties of the samples that became semiinsulating and improved their mobilities in relation to the starting semiconducting situation, table I.

The SPC map of sample A is shown in figure 24. The white line determines the edge of the electrodes. Only the inner area will be further considered for PC analysis. The photocurrent is homogenously distributed with variations about 15% around the mean value in contrast to as-grown SI-InP:Fe wafers that present photocurrent

24

fluctuation over 40%. Some local fluctuations appear modulating a relative flat background.

The SPC map of the sample B is shown in figure 25. In this case the photocurrent distribution is even more homogenous than it was for sample A. Relative variations below 10% are obtained. Local photocurrent fluctuations, similar to those reported for the other sample are also observed. These variations give a granular photocurrent pattern superposed to the smooth background. A slight gradient of the photocurrent is also observed on both samples. This gradient is more pronounced in sample A and might be the reason of the higher dispersion of the photocurrent. Grdients can be introduced by temperature gradients inside the furnace

Photoluminescence (PL) maps show for both samples a similar distribution as the one obtained by PC. The main observation is the absence of the growth striations. Figure 26 and 27 show PL maps of samples A and B respectively.

At high spatial resolution, the PL shows a characteristic granular distribution for both samples. However, the PL map of sample B presents a smoother contrast than sample A, See figures 26 and 27. These observations point out to a more homogenous distribution of electrically active Fe in sample B.

The difference between both samples was the cooling rate and the starting resistivity and mobility. The faster cooling rate was applied to B, which under standard thermally activated parameters of iron suggests a higher dispersion with lower iron concentration, contrarilly to what is really observed. Nevertheless, the starting electrical properties of the samples suggest an incomplete activation of iron in sample A as compared to sample B. A higher iron content in sample A than in sample B is possible, butwith a significant part of the iron in A electrically inactive. This inactive iron could be forming microprecipitates, which could be solved during the annealing step. The incomplete dissolution of the precipitates could account for the observed granular structure in sample A.

Close to the sample edges (left and right) both PL and PC are enhanced. Following the discusion of the previous paragrahps about the origin of the contrast in PL and PC maps we can conclude that these boundary regions are highly compensated and have a low iron concentration. This fact can be related to a more efficient shallow donor outdiffusion nearby the edges, which migrate to free surfaces and are eliminated. At the edge regions, free surfaces are available and therefore the annihilation of hydrogen complexes can be more efficient leading to a better compensation with less iron concentration, since iron also diffuses near the edges leaving an area parcially denuded of iron. A similar mechanism can be invoked near the crystal defects, which were found to give a similar behaviour as that reported herein, see the previous discussion about the iron distribution around crystal defects.

In fact, the properties of the wafers converted to semiinsulating by annealing of lightly Fe-doped InP show good homogeneity but seem to depend strongly of the properties of the starting material and in particular of the fraction of electrically active iron.

Annealing of Fe-doped semiinsulating InP

We can distinguish different annealing procedures for this type of material.

i.   Short time (a few hours) annealing at 950°C or above.

ii.   Long term wafer annealing

iii.   Long term ingot annealing

iv.   Multiwafer annealing

Method i mostly aims to remove stress. Additionally some improvement of the homogeneity is detected. We present herein results obtained by PL and PC mapping in ingot annealing Fe-doped InP supplied by Air Force Research Labs and grown and

26

processed by M/A COM. The ingots were 3 inch LEC. They were treated at 950°C during 6 hours. This short annealing time does not anneal out most of the inhomogeneities expected in this type of material, though it practically removes the strain.

The PL map of an (100) wafer is shown in Fig.28. The main features of the PL distribution are:

i. The PL pattern is arranged in concentric rings. The center exhibits a lower PL intensity. There is a large crown, which occupies the main part of the wafer and presents a good PL intensity homogeneity. The outer region exhibits low PL and appears very well defined.

ii. The radial doping growth striations are not observed.

The absence of the radial growth striations is surprising, since ingot annealing normally does not fully remove the doping growth striations (25) and in particular for a so short annealing time they must not be removed. The non-observation of the doping growth striations can obey different causes.

i. Effective iron redistribution in 3-inch ingot annealed Fe-doped InP. Up to now we handled only data concerning 2-inch ingots.

ii. Improved iron redistribution at 950°C compared to the conventional 900°C studied up until now.

In relation to this we note that the PL distribution is not the same of as-grown 2-inch Fe-doped InP wafers, see Fig.11, therefore further studies of as-grown 3-inch wafers would be value in order to understand the PL distribution in annealed 3-inch InP.

iii. The state of the surface can affect the PL measurement. The absence of the radial doping growth striations could be associated with the state of the surface, which was etched in this wafer. In fact, the PL intensity must be very sensitive to the state of the surface, since the PL arises only from the top surface, therefore surface damage play a main role in the PL response..

High resolution PL maps were obtained in the center and the medium crown of the wafer, Figs.29 and 30 respectively. They show a rough pattern, without vestiges of the growth striations. This rough pattern could be associated with the above mentioned state of the surface, since the typical brihgt PL spots are not clearly revealed.

A couple of (110) wafers from the ingot seed side were also studied. This part of the ingot is expected to have a lower iron concentration, due to the small distribution coefficient of iron, therefore, one can expect that the inhomogeneities related to the distribution of iron appears less marked in the central part and the tail of the ingot where higher iron amounts are incorporated. The PL map is shown in Fig.31. The axial growth striations are clearly observed, revealing the interface shape. They appear more spaced at the central part of the ingot, in the axial region. The luminescence intensity is observed to decrease around the crystal axis, which is in agreement with the observation of the low PL intensity in the center of the (100) wafer. However, the low PL intensity in the periphery is not so well observed in this part of the ingot, contrarilly to the observation reported for (100) wafer, it should be noted that in these wafers the periphery is in the cone region.

The observation of the doping growth striations in these wafers, that were optically polished, confirms the importance that the surface state has on the observation of PL fluctuations at a microscale.

High resolution PL maps were also obtained, Fig.32, showing the typical bright spots superposed to the growth striations distribution. These bright spots are associated with the gettering action of microdefects that under thermal treatment leave the surrounding area depleted of iron and hydrogen related donors, see the discussion about the PL and PC responses around crystal defects in the previous paragraphs. If this behaviour was a general trend of crystal defects, in annealed ones it is even more clear, since during the annealing step crystal defects getter both iron and donors, in particular the hydrogen related complexes. However, all the results obtained suggests that the outdiffusion of these complexes is faster than iron, which should account for overall resistivity increase after thermal treatment and in particular the enhanced PL and PC around crystal defects and the Cottreel atmosphere spread out observed in annealed

28

specimens. This mechanism will also explain the observed low PL at the periphery crown in the (100) wafer. In fact the annealing drives Hydrogen to the ingot periphery faster than iron, which increases $[Fe^{2+}]$, and thereafter the product $[Fe^{2+}]*[Fe^{3+}]$ with the corresponding decrease of the luminescence intensity. That this annealing, even so short induced the diffusion of hydrogen complexes is demonstrated by the improvement of the electrical properties, Fig. 33. The out-diffusion of iron is much less efficient as demonstrated by the permanence of the growth striations after this annealing, note that the distance between adjacent growth striations is a few μm's, which suggests that the effective diffusion distance of iron during the annealing step is smaller than the average distance between growth striations. In general, ingot annealing is not an efficient procedure to remove growth striations, unless it is done on wafers, were the homogenization is not done laterally, but by diffusion toward the top and the back surfaces of the wafers.

Photocurrent maps of these wafers were also obtained. Two samples were cut from the (100) and the (110) wafers respectively. The PC maps show anticorrelation with the PL intensity distribution. Note that we refer here to the long range inhomogeneities. The PC is enhanced in the axial region in wafer (100), then it decreases monotonically toward the edges, Fig.34, for a better observation scan profiles are are also shown in Fig.34. This behaviour is consistent with the expected anticorrelation between PL and PC, however, this anticorrelation does not take place at the edge of the wafer, where both PL and PC are decreased. This behaviour could be explained assuming a high $[Fe^{2+}]$ concentration in that area, which would give low compensation ratio, $[Fe^{3+}]/[Fe^{2+}]$, and high $[Fe^{3+}]*[Fe^{2+}]$. However, this is inconsistent with the resistivity profile measured in a wafer of the same ingot, Fig.33, that shows a resistivity enhancement at the wafer edge. This observation rules out the previous hypothesis of a low compensation ratio. Then a possible explanation for this behaviour could be the reduction of the mobility at the wafer edge. This is confirmed by the mobility profile, Fig. 33, which evidences a decrease at the wafer edge.

A sample of wafer (110) was also cut and the photocurrent map was observed, Fig.35. The anticorrelation between luminescence and photocurrent at the axial region is also confirmed. Note the photocurrent pattern parallel to the cleaved side. The

29

photocurrent is enhanced and this enhancement seems to be related to the cleveage. It suggests an influence of stress on the photocurrent intensity, Remind that the photocurrent distribution of as-grown wafers, Fig.14, revealed the characteristic fourfold symmetry of the stress distribution in LEC ingots. The relation between stress distribution and the photocurrent response will be the object of a specific study in the future.

Annealing methods ii and iii were discussed in a previous work (25). The results obtained by those annealing procedures can be basically summarized as follows:

Wafer annealing gives better homogeneity than ingot annealing, however, the ingot annealing has advantages in terms of time and cost. Also, the high brittelness of InP, would give advantage to the ingot annealing process. According to this and the fact that stress is released by the procedure i, one possible routine could be a short ingot anneling and then subsequent wafer annealing. The annealing parameters giving the best conditions in terms of electrical properties and homogeneity were selected from this analysis: $T_{ann}>900°C$, $t_{ann}>50$ h, cooling rate=$30°C$, Phosphorous overpressure<2 bar.

Finally, the fourth annealing method is the multiwafer annealing. It has got very good results to improve GaAs wafers and it was also developped for InP, though it was not studied in this report.

Doping semiconducting InP by iron diffusion.

The keys for the actual improvement of the semiinsulating InP substrates are on one side the significant improvement of the as-grown material and on the second hand the optimisation of the thermal treatments. In spite of this, we have to consider the axial gradient of the iron distributuion. While the wafer homogeneity can be optimised by adequate thermal treatments, the axial distribution cannot be so done. This constitutes a strong drawback to obtain wafers of similar characteristics from an ingot.

An alternative route to avoid the axial gradients is the doping of semiconducting InP by annealing the wafers in the presence of an iron source. We present herein some results concerning this method. Undoped InP wafers with standard electrical characteristics ($n \approx 5 \times 10^{15}$ cm^{-3}, $\mu = 4400$-4700 cm^2/Vs) were used for this treatment. A thin Fe layer was deposited on the wafer surface. Then they were annealed at 900°C for 50 hours. Hall effect measurements showed that the wafers become semi-insulating with resistivities well above 10^7 Ω–cm and mobilities in the range 3000-4000 cm^2/Vs after this treatment.

The electrical characterisation indicates that the Fe-diffused wafers have electrical properties generally better than those of the standard as-grown Fe-doped LEC InP. The resistivity and mobility are high despite the low Fe concentration, which implies a high compensation ratio. Note that high resistivity and high mobility were possible only in as grown semiinsulating Fe-doped InP materials where the ratio ($[Fe^{3+}]+[Fe^{2+}]$) /$[Fe^{2+}]$ was $>= 2$.

Mass spectroscopy analysis gave a total Fe content, after Fe diffusion of about 4.5×10^{15} cm^{-3}, which leads to conclude that the concentration of shallow donors is strongly reduced from the initial value to less than 2×10^{15} cm^{-3}. From these estimations one can deduce that the great majority of the diffused Fe atoms seem to be electrically active, in contrast to the case of as-grown LEC InP where the fraction of active Fe is about 0.3-0.7 of the total.

Photoluminescence (PL) mapping shows that the uniformity of the Fe-diffused InP wafer is good, Figure 36. It should also be noted that the iron diffused wafers are uniform on a microscale and that only the wafer rim shows significant changes of PL intensity.. It is important to note that the PL intensity is higher close to the flat, where the resistivity was observed to be higher. This is consistent with the fact that the intrinsic PL intensity is not only inversely proportional to the electrically active iron concentration [13], but it is also governed by the $[Fe^{2+}]$ in the sense that it increases when $[Fe^{2+}]$ decreases and viceversa. Therefore, the high resistivity and the high PL intensity are in perfect agreement if one assumes that the increase of the

31

$([Fe^{3+}]+[Fe^{2+}])/[Fe^{2+}]$ ratio is mostly due to a decrease of the shallow donor concentration. The asymmetry of the PL distribution is rather probably the consequence of a temperature gradient in the furnace. In other words, the different temperature between different parts of the wafer will result in variations of the compensation ratio $([Fe^{3+}]+[Fe^{2+}])/[Fe^{2+}]$ across the wafer.

Regarding the uniformity on the microscale a high-resolution PL map of Fe-diffused InP is shown in fig. 37. The homogeneity of the sample is very good as there are no traces of Fe gettering around dislocations. It should be remembered that in as-grown Fe-doped InP the dislocations are very often decorated by Fe-rich particles while the volume around them is depleted. However, bright spots are not observed in these iron diffused wafers. Despite the linear structures associated with scratches produced during handling, the PL homogeneity is far better than that normally found in InP where the Fe is introduced into the melt before growth. In this case, both growth striations and effects associated with dislocation structures are very prominent. However, these PL features are totally absent in the Fe-diffused material.

The iron diffused samples were also mapped by photocurrent. Figure 38 shows the PC map of a quarter of an iron diffused wafer. It should be noted that, apart the sample rim, which is affected by the measurement electrodes, the PC signal throughout the sample is relatively uniform, though the typical fourfold symmetry is guessed, which rises once agin the role of the strain distribution in the compensation ratio distribution.. This suggest that the concentration of iron in the bulk of the wafer is also homogeneous and the fourforld asymmetry typical of as-grown Fe-doped InP is not observed.

REFERENCES

1 S.G.Bishop; "Deep Centers in Semiconductors", ed. by S.T. Pantelides (Gordon and Breach, New York 1986) Ch.8

2. G. Bremond, A. Nouailhat, G. Guillot, B. Cockayne; Electron. Lett. 17, 55 (1981)

3 P.R. Tapster, M.S. Skolnick, R.G. Humphreys, P.J. Dean, B. Cockayne, W.R. MacEwan; J.Phys. C 14, 5069 (1981)

4. D.C. Look; Phys. Rev. B 20, 4160 (1979)

5. G.C. Valley, S.W. McCahon, M.B. Klein; J.Appl. Phys. 64, 6684 (1988)

6. S.Asada, S.Sugou, K.I. Kasahara, S. Kumashiro; IEEE J.Quantum Electron. QE-25, 1362 (1989)

7. A.E. Iverson, D.L. Smith, N.G. Paultier, R.B. Hammond; J.Appl. Phys. 61, 234 (1986)

8. D.Soderstrom, S. Markenvicius, S.Karlson, S.Lourdudoss; Appl. Phys. Lett. 70, 3374 (1997)

9. T.Takanohashi and K.Nakajima; J. Appl. Phys. 65, 3933 (1989)

10. G.Lukovsky; Solid St. Commun. 3, 299 (1965)

11. K.Tonkhe, K. Pressel; Phys. Rev. B 44, 13418 (1991)

12. K. Pressel, K.Tonkhe, A.Dornen; G.Pensl; Phys. Rev. B 43, 2239 (1991)

13. O. Oda, K. Kainosho, K. Kohiro, H. Shimakura, T. Fukui, R. Hirano and S. Katsura; Proc. 6th Intern. Conf. on Semi-insulating III-V Materials, Toronto 1990, Eds. A. Milnes and C. Miner, IOP Bristol 1990, p. 189

14. W. Meier, H.Ch.Alt, Th. Vetter, J.Volkl and A. Winnacker; Semicond. Sci. Technol. 6, 297 (1991)

15. G.Muller; Phys. Scr. 35, 201 (1991)

16. G.Hirt, D.Wolf, B.Hoffmann, U.Kretzer, G.Kühnel, A.Woitech, D.Zemke, G.Müller; J.Electron. Mater. 25, 363 (1996)

17. D. Wolf, G.Hirt, F. Mosel, G.Muller, J. Volkl; Mater. Sci. Eng. B28, 115 (1994)

18. R. Fornari; J. Electron. Mater. 20, 1043 (1991)

20. R. Darwich, B.Pajot, B.Rose, D.Robein, B.Theys, R.Rahbi, C.Porte, F.Gendron; Phys. Rev. B 48, 17776 (1993)

21. D.F.Bliss, G.Bryant, D.Gabbe, G.Iseler, E.E.Haller and F.X.Zach; Proc. of 7th

Int. Conf. on InP and Rel. Mater., Sapporo 1995, IEEE Catalog No. 95CH35720, p.678

22. M.Avella, J.Jiménez, A. Alvarez, M.A. Gonzalez, L.F.Sanz; Mater. Sci. Eng. B 28, 111 (1994)

23. A. Alvarez, M. Avella, J.Jimenez, M.A. Gonzalez and R. Fornari; Semicond. Sci. Technol. 11, 941 (1996)

24. L.F. Sanz, M.A. Gonzalez, M. Avella, J. Jimenez and R.Fornari; Materials Science Forum 258-263, 825 (1997)

25. M.Avella, J.Jiménez, A.Alvarez, R.Fornari, E.Gilioli, A.Sentiri; J.Appl. Phys. 82, 3832 (1997)

26. J.Jiménez, R.Fornari, M. Curti, E. de la Puente, M.Avella, L.F. Sanz, M.A. Gonzalez, A.Alvarez; MRS Symp. Proc. 484, 625 (1998)

27. J.Jimenez, R. Fornari; Defect Diff. Forum (Pt.A) 157-159, 103 (1998) 103

28. P.B.Klein, J.E.Furneaux, R.L.Henry; Phys. Rev. B 29, 1947 (1984)

29. J.Y.Longere, K. Schohe, S.Krawczyk, R.Coquille, H.L'Haridon and P.N. Favennec; J.Appl.Phys. 68, 755 (1990)

30. P.B.Klein, H.R.Henry, T.A.Kennedy and N.D.Wisey, in "Defects in semiconductors", Ed. H.J. von Bardeleben, Mater. Sci. Forum 10-12, 1259 (1986)

31. O.Oda, K.Kainosho, K.Kohiro, R.Hirano, H.Shimakura, T.Inoue, H.Yamamoto, T.Fukui; J.Electron. Mater. 20, 1007 (1991)

32. G. Hirt, D. Hofmann, F. Mosel, N. Schäfer and G. Müller; J. Electron. Mater. 20, 1065 (1991)

33. O. Oda, H. Yamamoto, K. Kainosho, T. Imazumi and H. Okazaki; Proc. of DRIP 5, Ed. J. Jimenez, Inst. Phys. Conf. Ser. 135, IOP, Bristol 1994 p. 288

34. G. Hirt, D. Wolf and G.Müller; Proc. of Semi-Insulating III-V Materials, Warsaw 1994, Ed. M. Godlewski, World Scientific Publ., Singapore 1994, p. 19

35. R. Fornari, B. Dedavid, A. Sentiri and M. Curti; Proc. of Semi-Insulating III-V Materials, Warsaw 1994, Ed. M. Godlewski, World Scientific Publ., Singapore 1994, p. 35

36. G. Hirt, T. Mono, G. Müller; Proc. of Semi-Insulating III-V Materials, Warsaw 1994, Ed. M. Godlewski, World Scientific Publ., Singapore 1994 p. 101,

37. K. Kainosho, M. Ohta and O. Oda; Proc. 7th Intern. Conf. on InP and Related Materials, Sapporo 1995, IEEE Catalog 95CH35720, p. 37

38. R.Hirano, M.Uchida; J.Electron. Mater. 25, 347 (1996)

FIGURE CAPTIONS

Fig.1. Optical cross sections of Fe levels (from 9)

Fig.2. Resistivity profiles across a wafer diameter for three wafers with different Iron contents (from 17)

Fig.3. Resistivity vs compensation ratio. Note the incidence of the variation of the compensation ratio on the resistivity fluctuations. (from 17).

Fig.4. PL experimental set-up.

Fig.5. PC experimental set-up.

Fig.6. PL numerical solution. I_{PL} vs $[Fe_{In}]$ for different $[Fe^{2+}]$

Fig.7. PC numerical solution. I_{PC} vs $[Fe_{In}]$ for different $[Fe^{2+}]$

Fig.8. The plots represented are the $[Fe^{2+}]$ vs $[Fe^{3+}]$ for constant I_{PL} and I_{PC} values. The data were numerically obtained solving the two set of rate equations describing PL and PC. Within the cross the signs + and - represent the evolution of the PL and PC, plus means that they increases and - means a decrease. This can be associated with the evolution of the PL and PC when the position across the wafer changes. In fact if the evolution is such that both correspond to the region with a + sign or a - sign, they are correlated, while if they have oppsite signs they would appear anticorrelated.

Fig.9. $[Fe^{2+}]$ vs $[Fe^{3+}]$ for different constant PC values, the three plots are the numerical solution, the anlytical solution and the $[Fe^{2+}]/[Fe^{3+}]$ ratio. Note the fair agreement between the three curves, which allows to relate the PC fluctuations to $[Fe^{2+}]/[Fe^{3+}]$ variations.

Fig.10. $[Fe^{2+}]$ vs $[Fe^{3+}]$ for constant PL, the three plots are the numerical solution, the anlytical solution and the $[Fe^{2+}] * [Fe^{3+}]$ ratio. The agreement shows that the PL fluctuations can be interpreted in terms of the variations of the $[Fe^{2+}] * [Fe^{3+}]$ product.

Fig.11. PL map of an as-grown wafer showing the rings characteristic of doping growth striations.

Fig. 12. Local bright PL spots.

Fig.13. PL image of a bright spot, showing the expected distribution around a grown-in dislocation.

Fig.14. PC maps of half as-grown wafer showing the typical fourfold distribution. Excitation a)with white light, b) with 1.06 light.

Fig.15. Crystal defect revealed by DSL, as observed by SEM, CL and PSM. The step profile revealing the etching rate, is also shown.

Fig.16. Crystal defect revealed by DSL, as observed by SEM, CL and PSM, a step profile is also shown.

Fig.17. Defect observed by SEM and CL. Note the reverse contrast in this case.

Fig.18. 3D view and calculated image obtained by PSM of a crystal defetct revealed by DSL

Fig.19. PL image of the front and the backside of a 350 μm thick sample. The two images were glided along the diagonal in order get the corresponding fringes into coincidence. This distance gives an idea of the inclination of the vertical curvature of the striations and accounts for their non observation in the PC maps.

Fig.20. a) Photocurrent scan of an old iron doped wafer, b) Photocurrent scan of an actual iron doped wafer

Fig.21. High resolution PC map of an as-grown wafer, top view and 3-D.

Fig.22. PC and PL maps of a crystal defect (see the Nomarski image of the DSL revealed defect). Note the correlation between the PL and PC intensities. This correlation suggests a high compensation ratio and a low electrically active iron concentration.

Fig.23. Resistivity vs iron concentration for annealed and Fe-doped InP

Fig.24.Photocurrent map of sample A

Fig.25. Photocurrent map of sample B

Fig.26. PL map of sample A

Fig.27. PL map of sample B

Fig.28. PL map of an annealed 3-inch wafer (InP 55). See the concentric distribution and the absence of growth striations. The homogeneity is good as compared to as-grown specimens. The absence of the growth striations can arise from the state of the surface.

Fig.29. High resolution PL map of aregion selected in the midcrown (red in Fig.18) of the same wafer of Fig.18. Note the absence of the growth striations and the rough PL distribution, which is probably due to the surface treatment, it was etched.

Fig.30. High resolution PL image of the central part of the wafer of Fig.18. The 3-D view is also included showing the typical PL distribution of the bright spots in Fe-doped InP (see ref. 29)

Fig.31. Pl map of the (110) wafer (InP 55) cut on the top of the ingot. Note the presence of the growth striations, which are not removed by the heat treatment. The observation of these growth striations confirms that they were not observed in the (100) wafer because of the surface treatment.

Fig.32. High resolution PL map othe (110) wafer showing large bright spots, which are associated with low iron content due to the gettering by the crystal defects. These structures are rather probably depleted of residual donors.

Fig.33. Electrical parameters obtained by Hall effect along a wafer diameter..

Fig.34. PC map of a slab cut along the < 011> direction of wafer 55, and PC profile along a diameter.

Fig.35. PC map of a sample cut from (110) wafer. Also a line scan is shown.

Fig.36. PL map of a Fe-diffused wafer.

Fig.37. High resolution PL image obtained on a Fe-diffused wafer.

Fig.38. PC map of quarter wafer diffused with iron.

TABLE CAPTIONS

Table I. Electrical data before and after annealing of samples lightly doped with iron.

Sample (wafer)	Annealing (cool. rate)	Resistivity (Ωcm)	Mobility (cm^2/Vs)	Hall conc (cm^{-3})
A	Before	14.58	3050	1.4×10^{14}
	After (30°C/h)	8.1×10^7	3860	1.9×10^7
B	Before	36.9	1076	1.5×10^{14}
	After (50°C/h)	8.0×10^7	2000	3.9×10^7

Table I
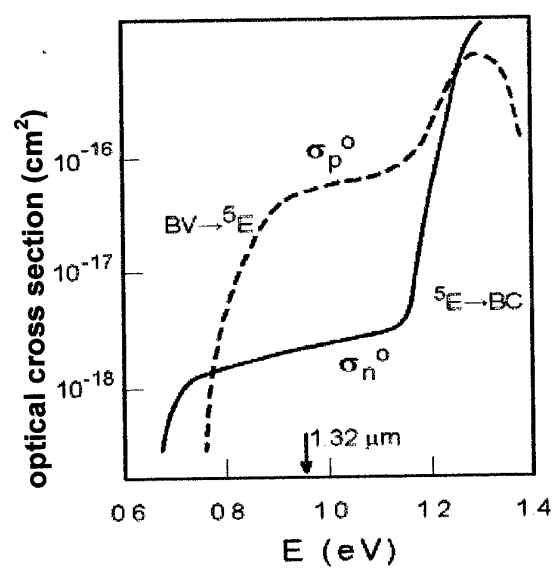
Fig.1
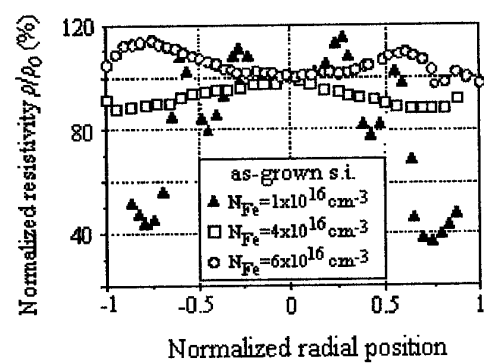
Fig.2
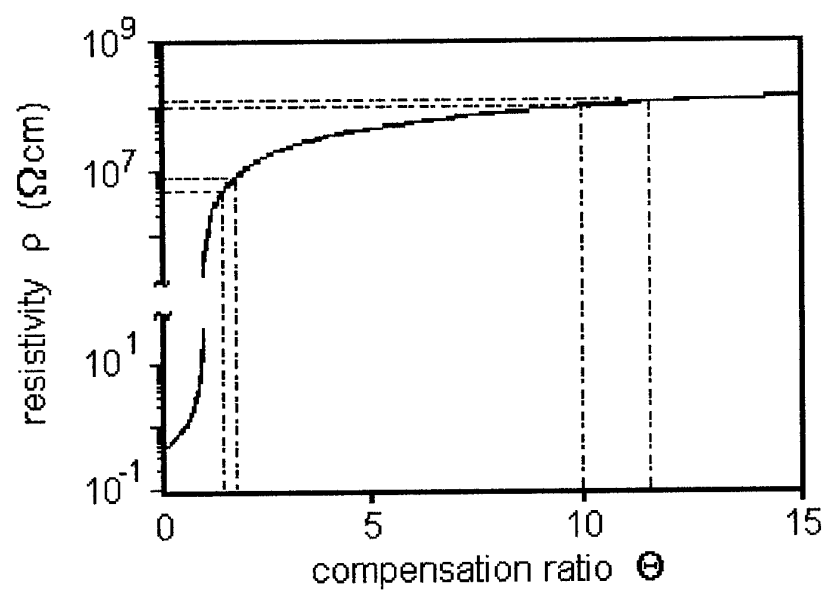
Fig.3
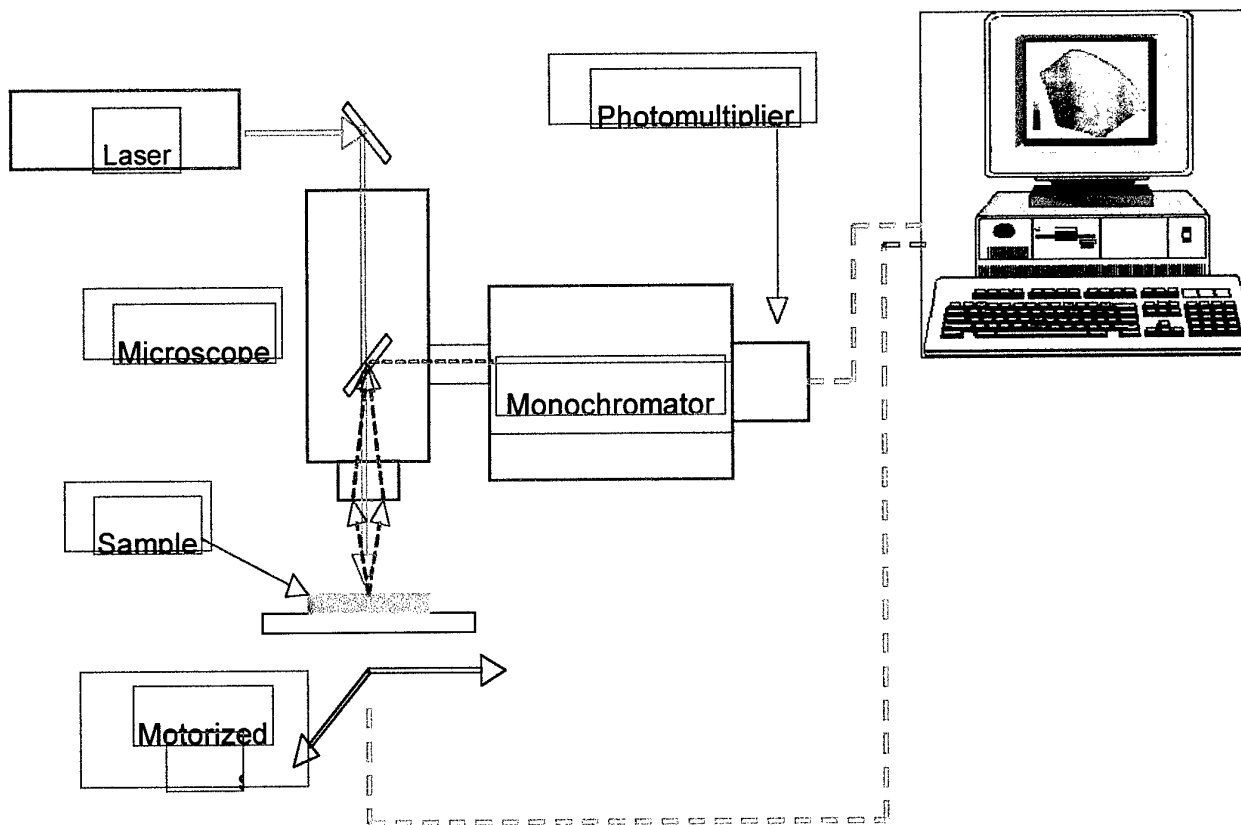
Fig.4
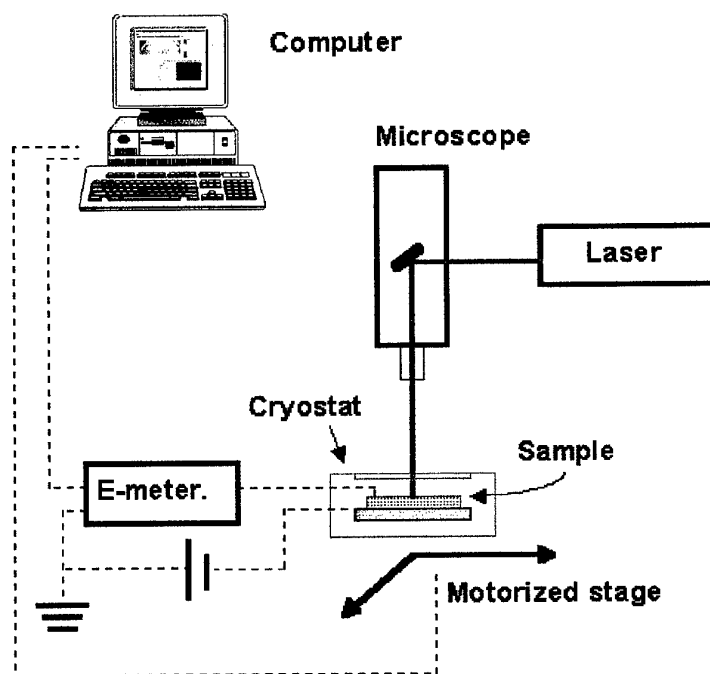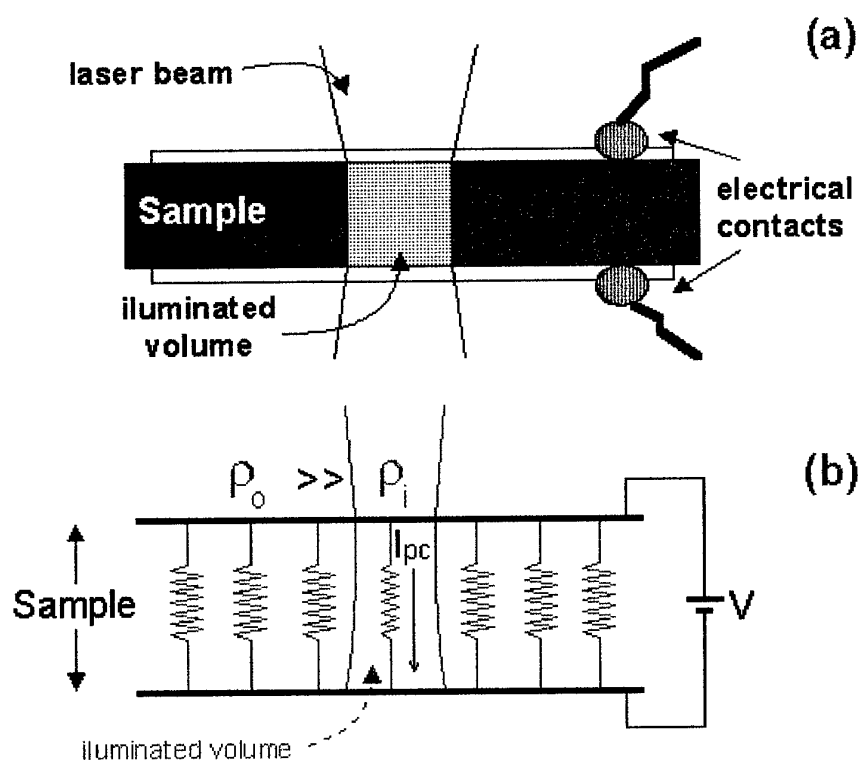
Fig.5
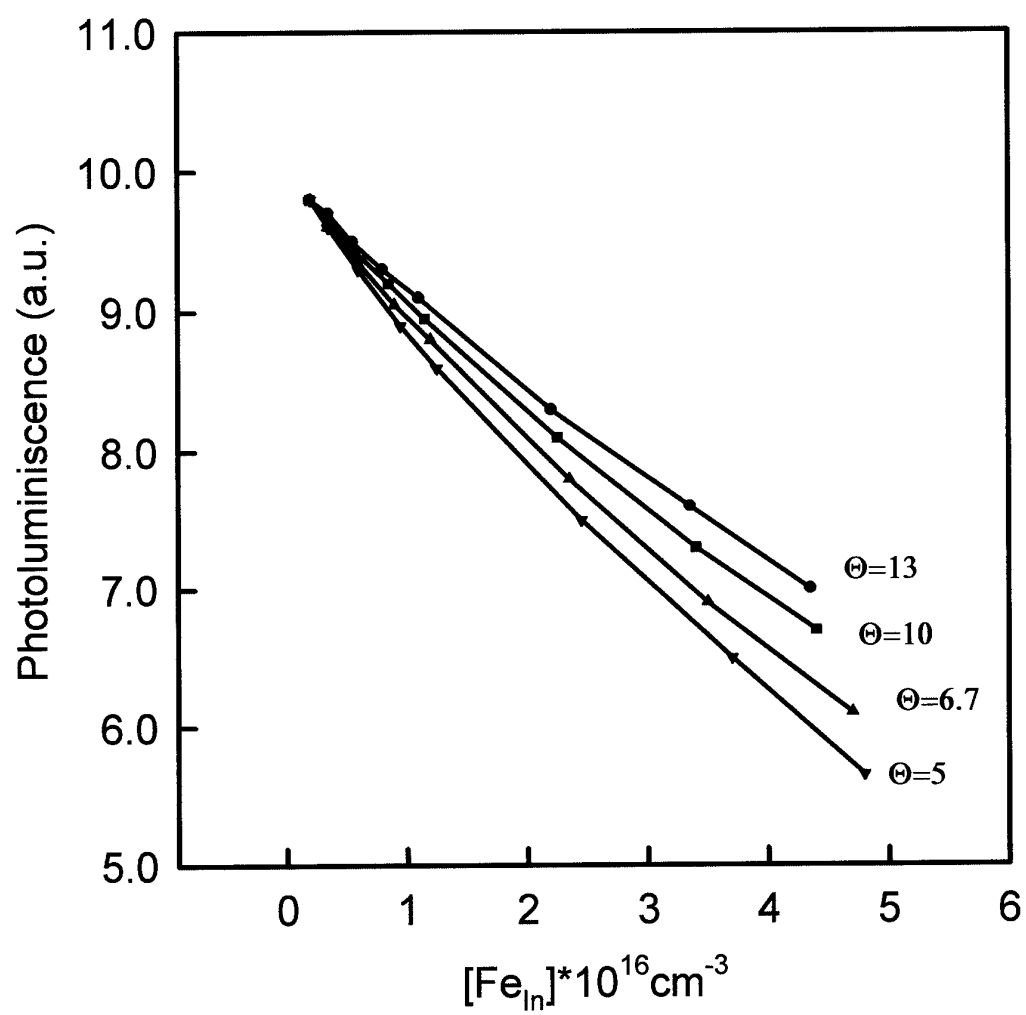
Fig.6
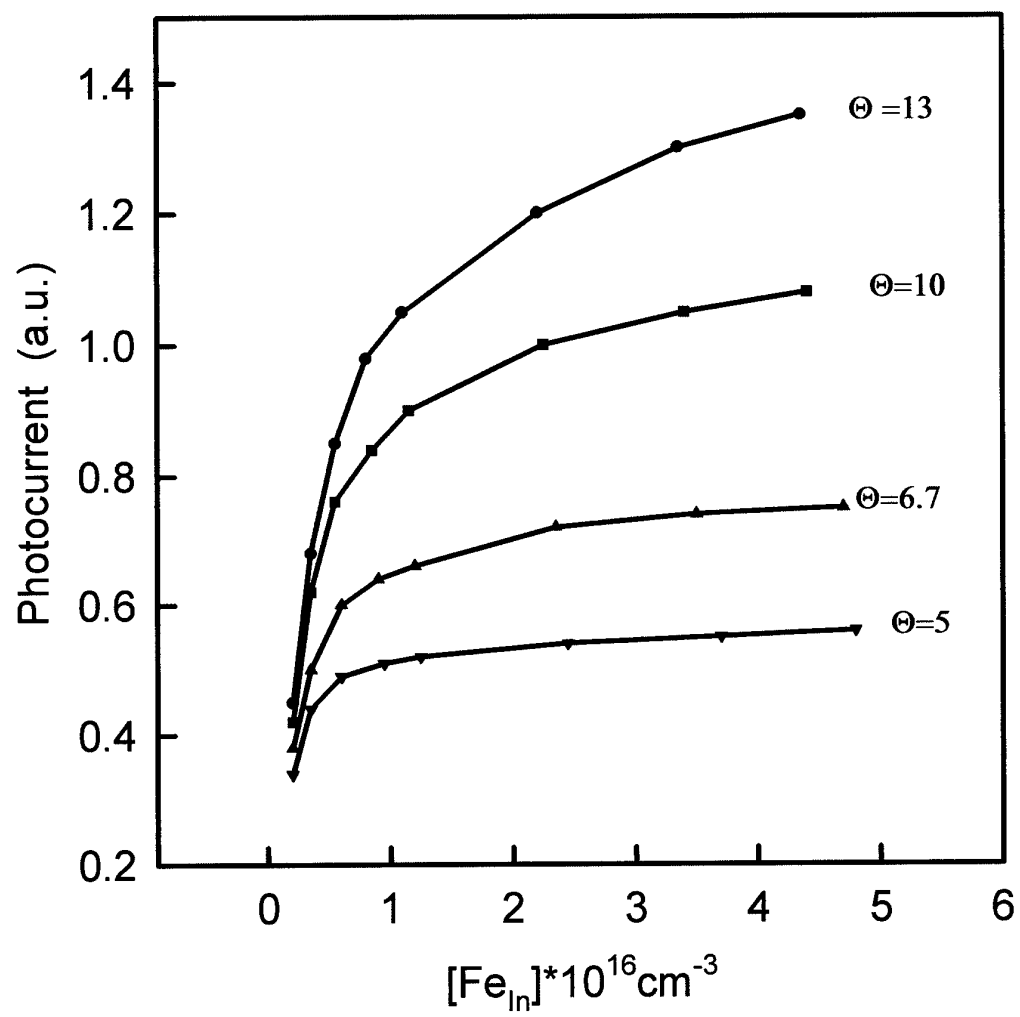
Fig.7
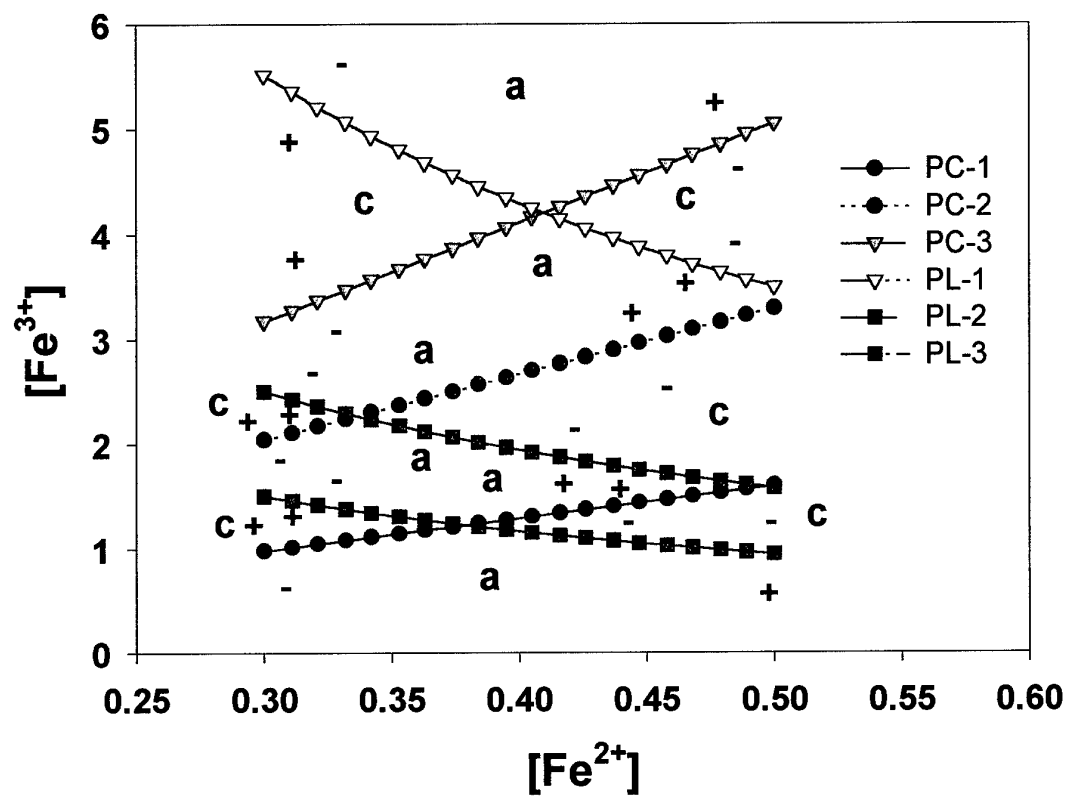
Fig.8
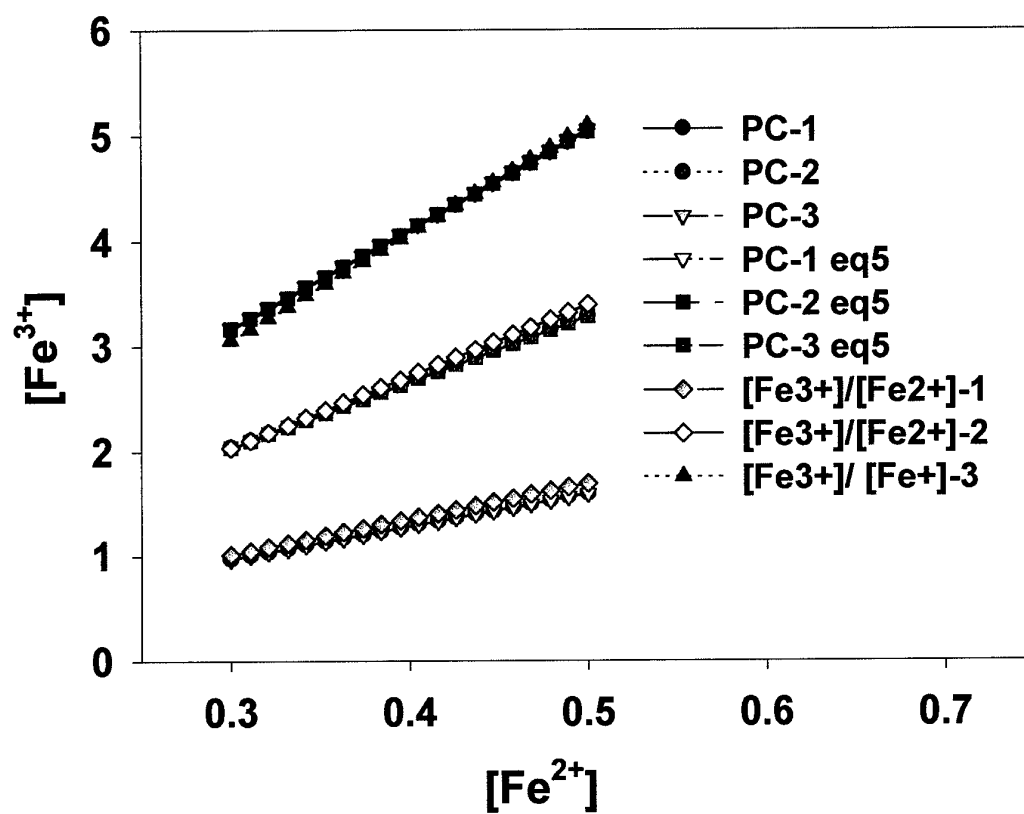
Fig.9
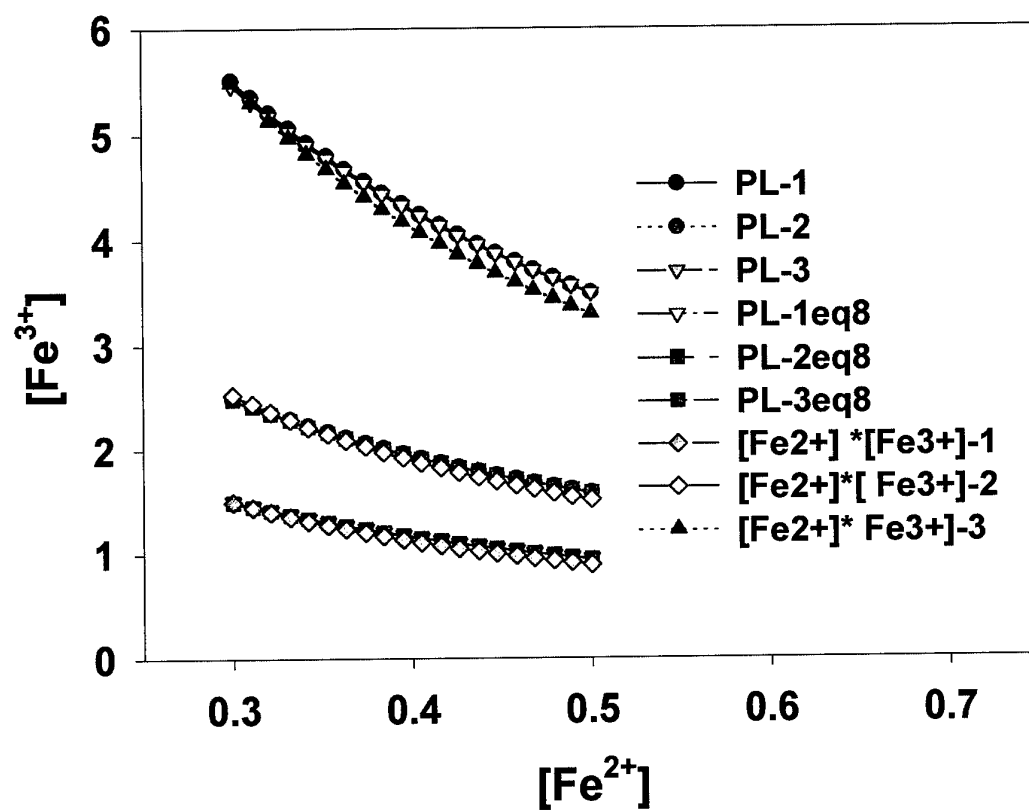
Fig.10
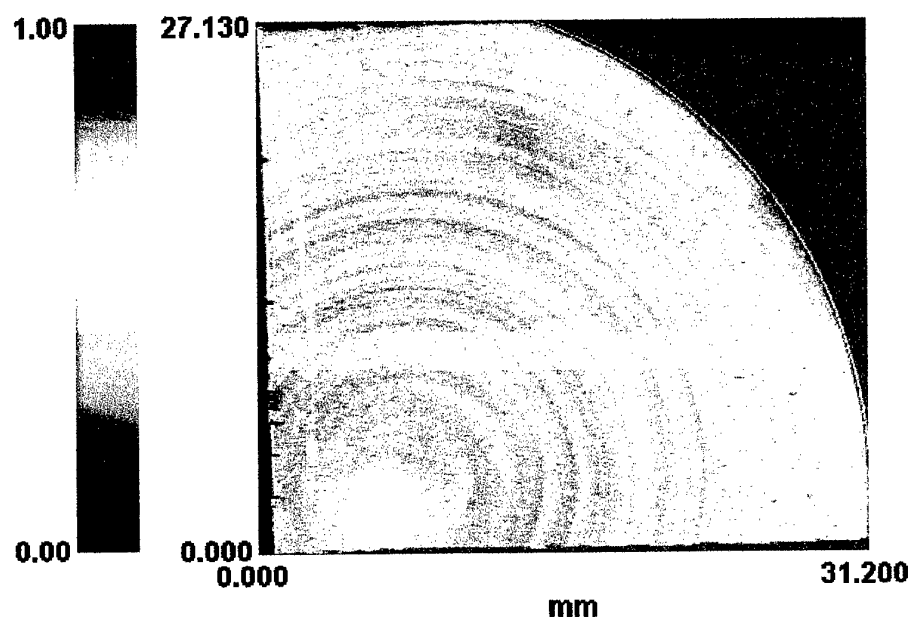
Fig.11
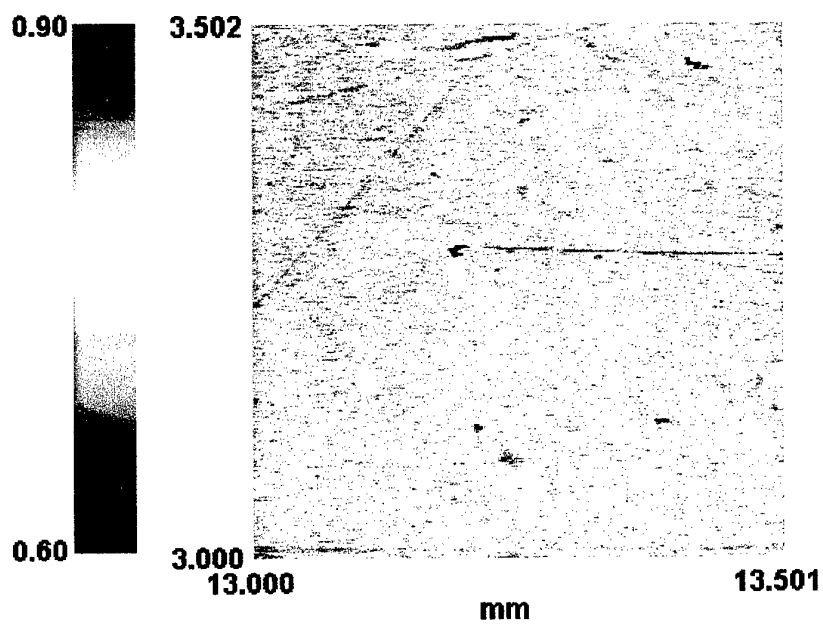
Fig.12
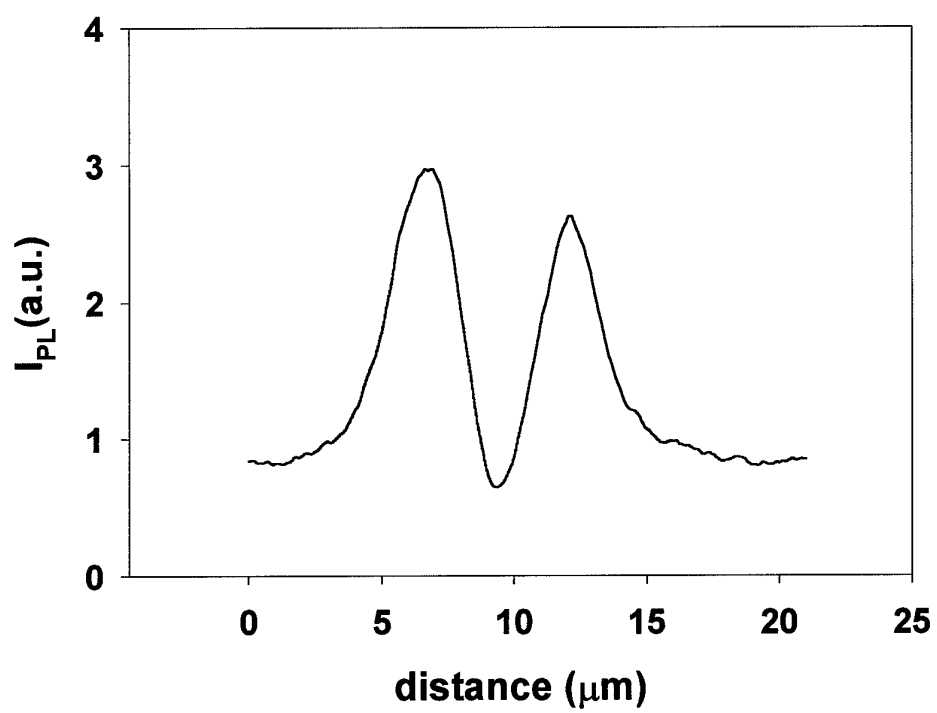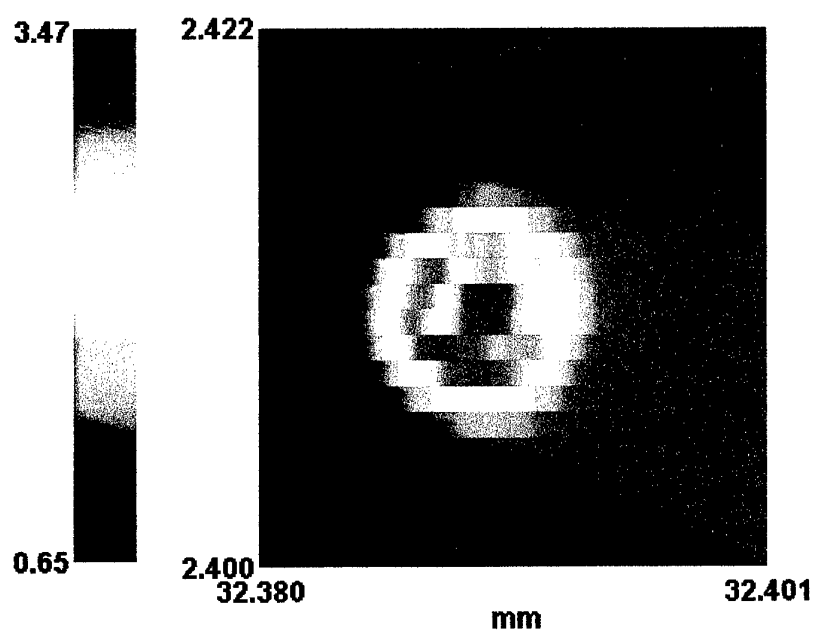
Fig.13
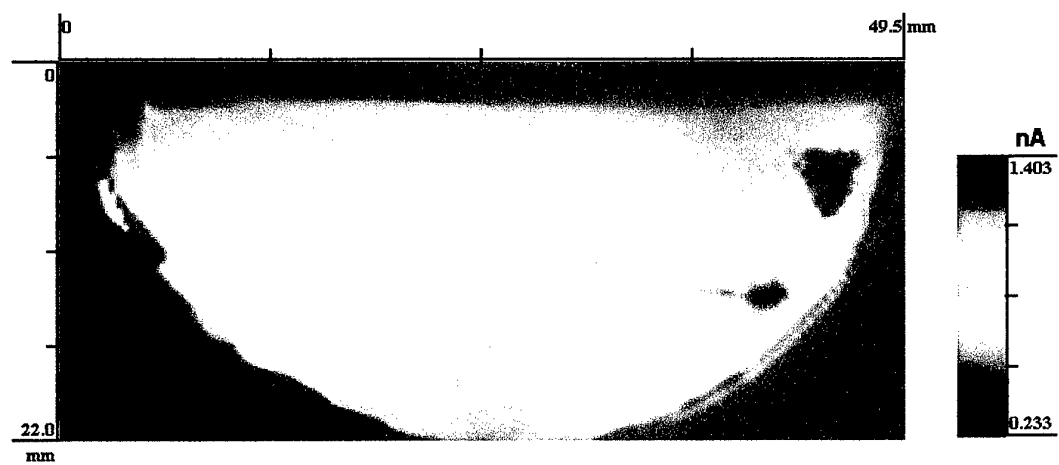
Fig.14

Label: W21,x2000,80K,SEM,im2
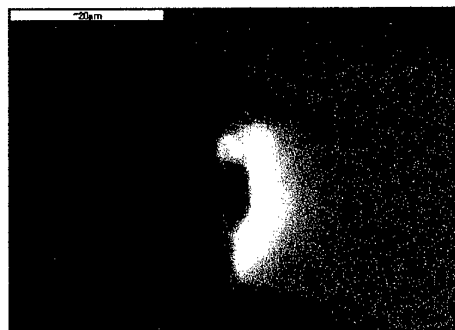
Label: W21,x2000,80K,panIR,img2

PSM image and profile of img2
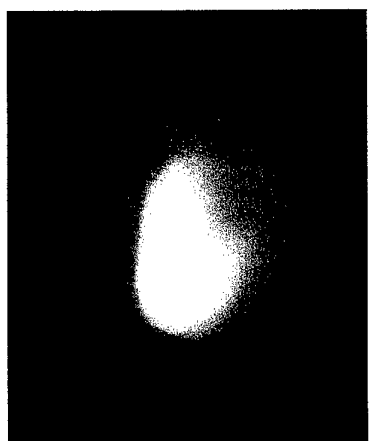
W21-img2CL-horizontal section
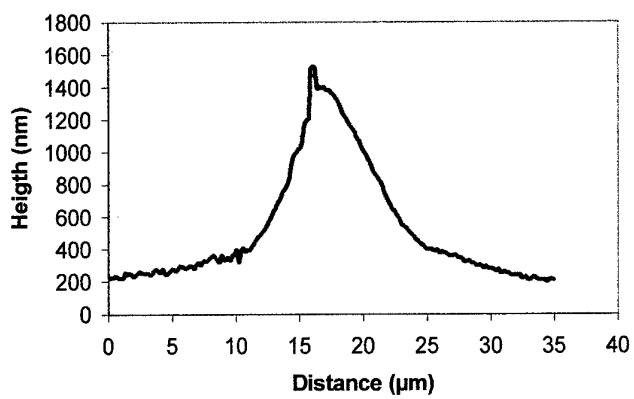
Fig.15

Label: W21,x3500,80K,SEM,img5

Label: W21,x3500,80K,panIR,img5
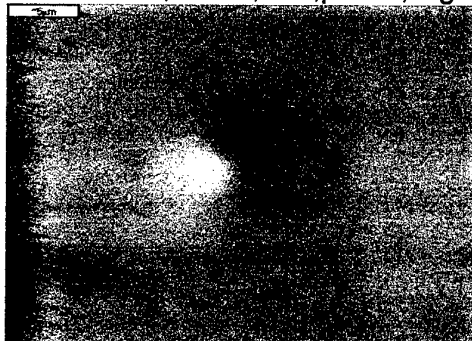
PSM image and profile of img5
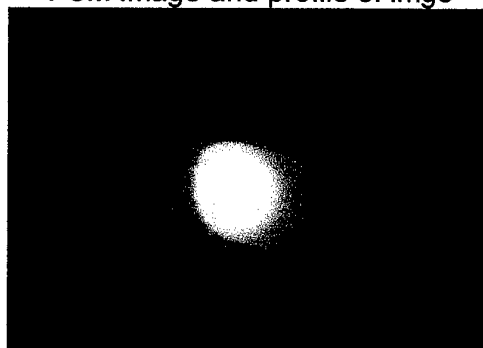
W21-img5CL-horizontal section
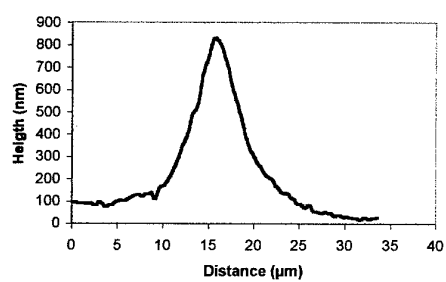
Fig.16

Label: W21,x6000,80K,SEM,img7

CL panchromatic image
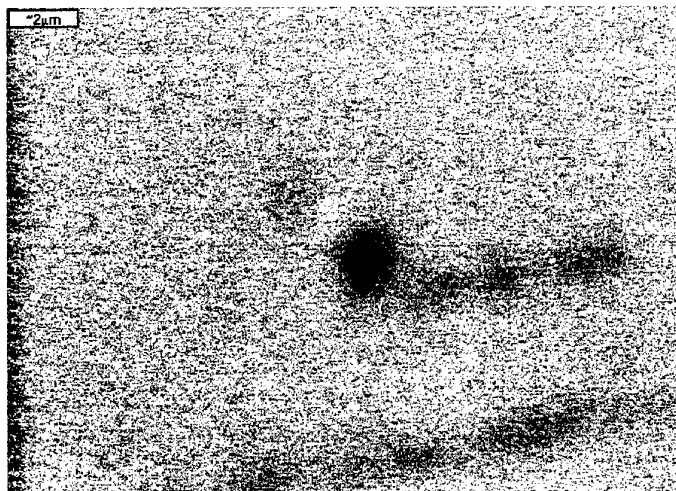
Fig.17

PSM3
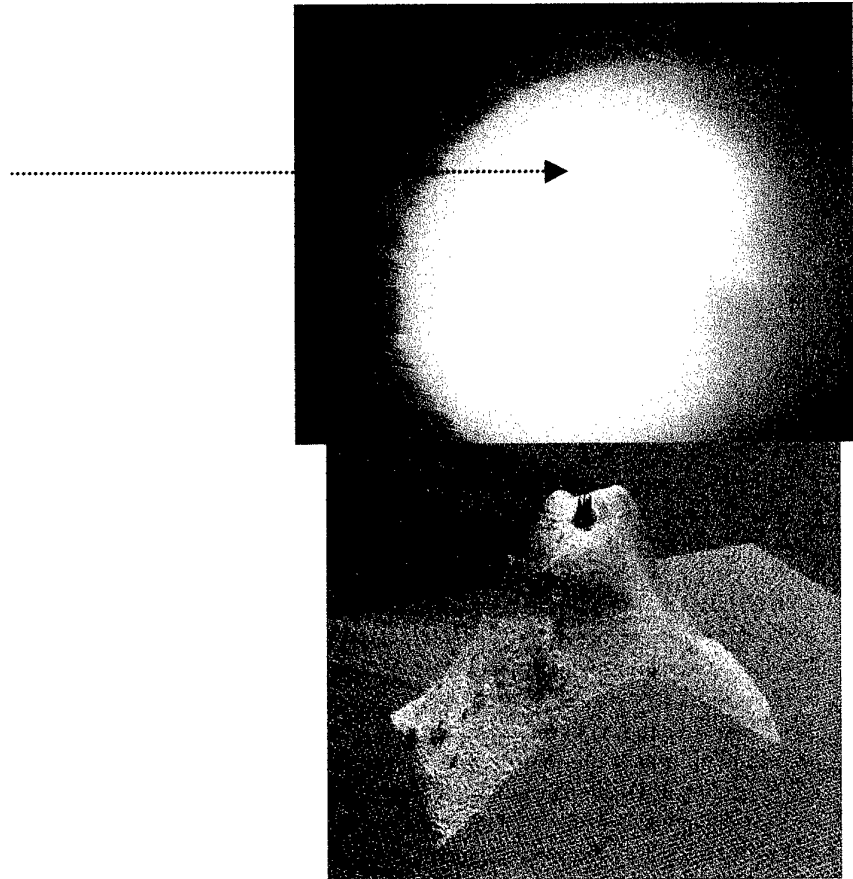
W21-psm3-horizontal section

Fig.18

Cara (B)

Cara (A)
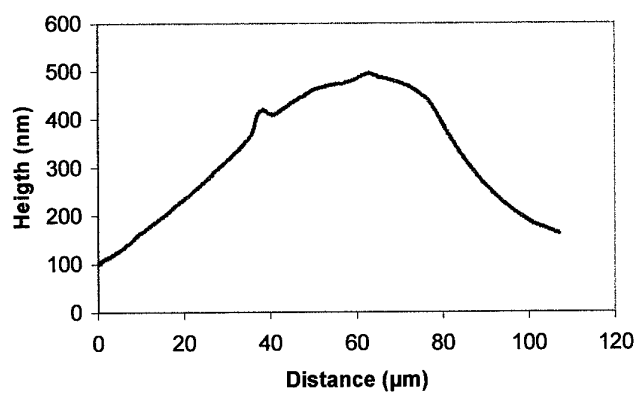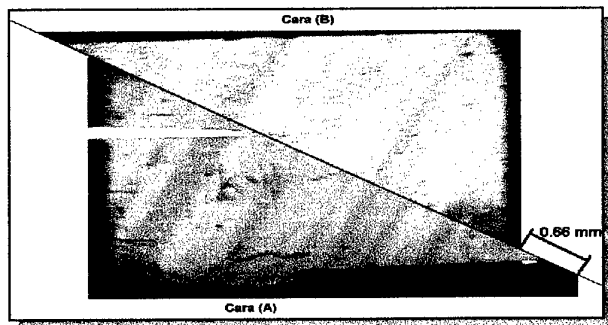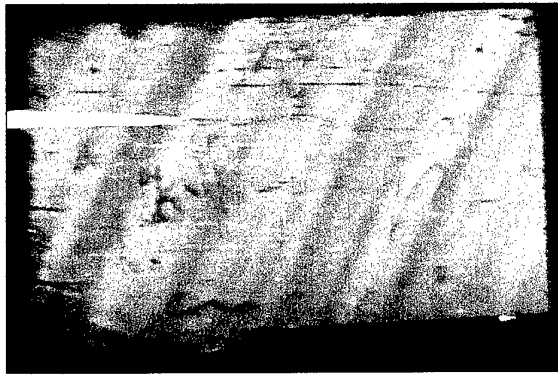
0.66 mm

Wafer thickness = 0.35 mm
Striations displacement = 0.66 mm

$$\frac{L_1}{L_2} = \frac{0.66}{0.35}$$

InP ingot

L_2

L_1
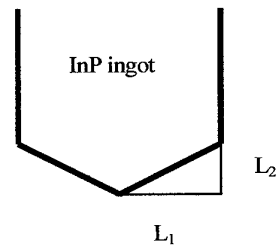
Fig.19
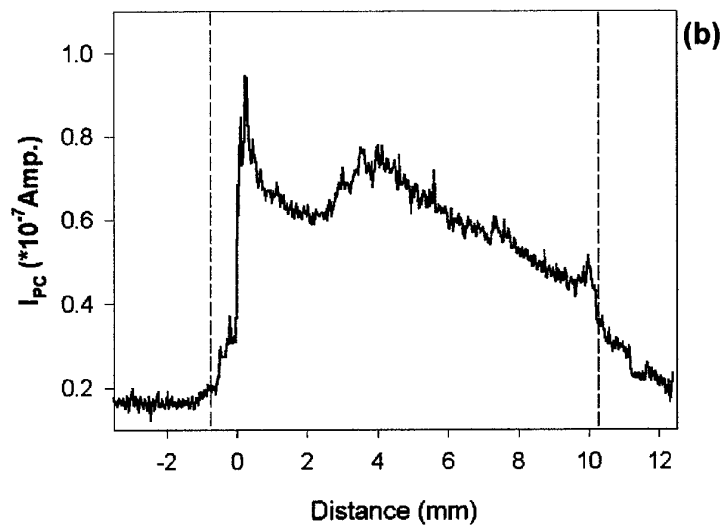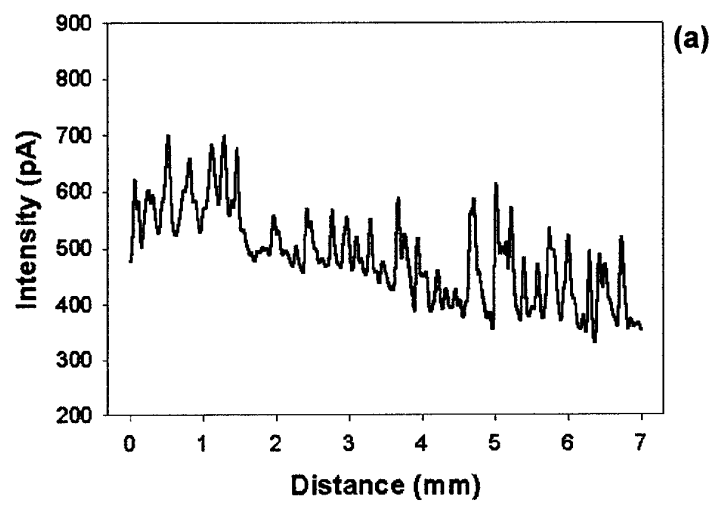
Fig. 20
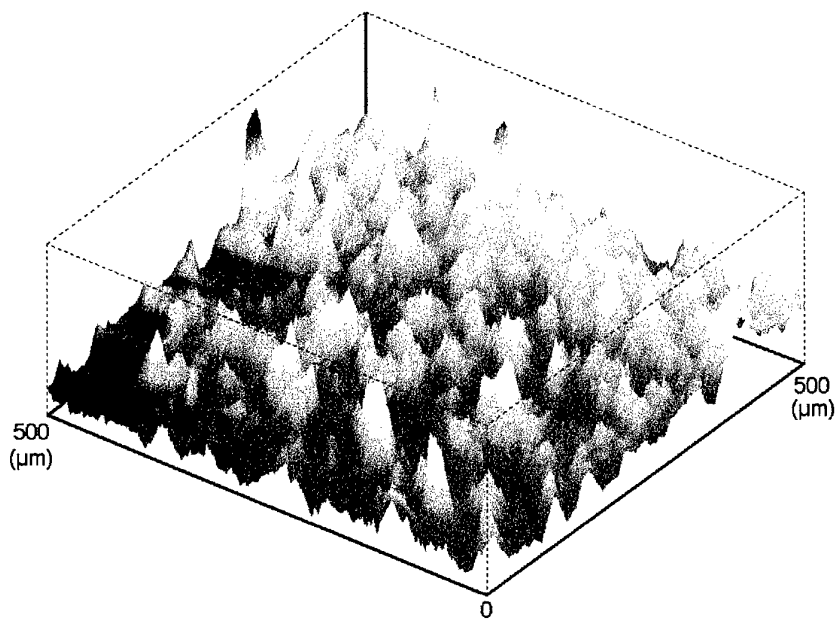
Fig.21
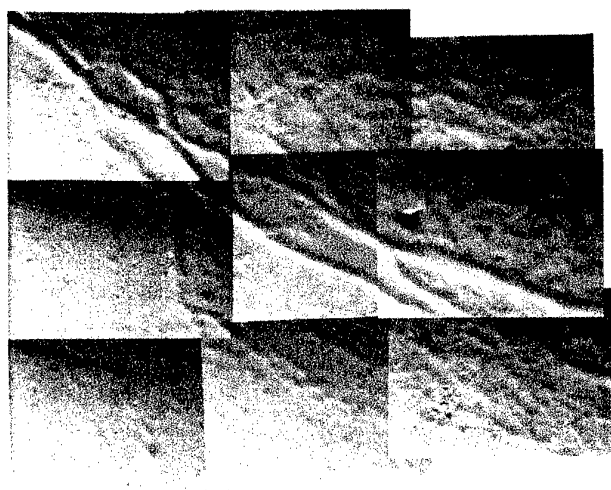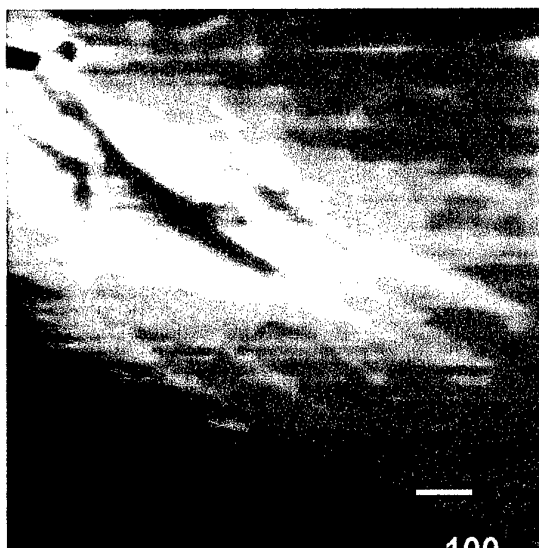
Fig.22
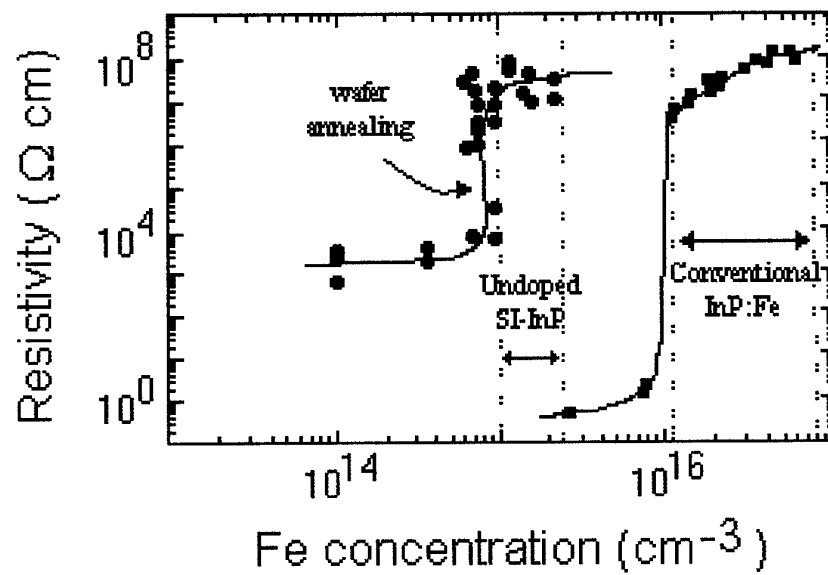
Fig.23
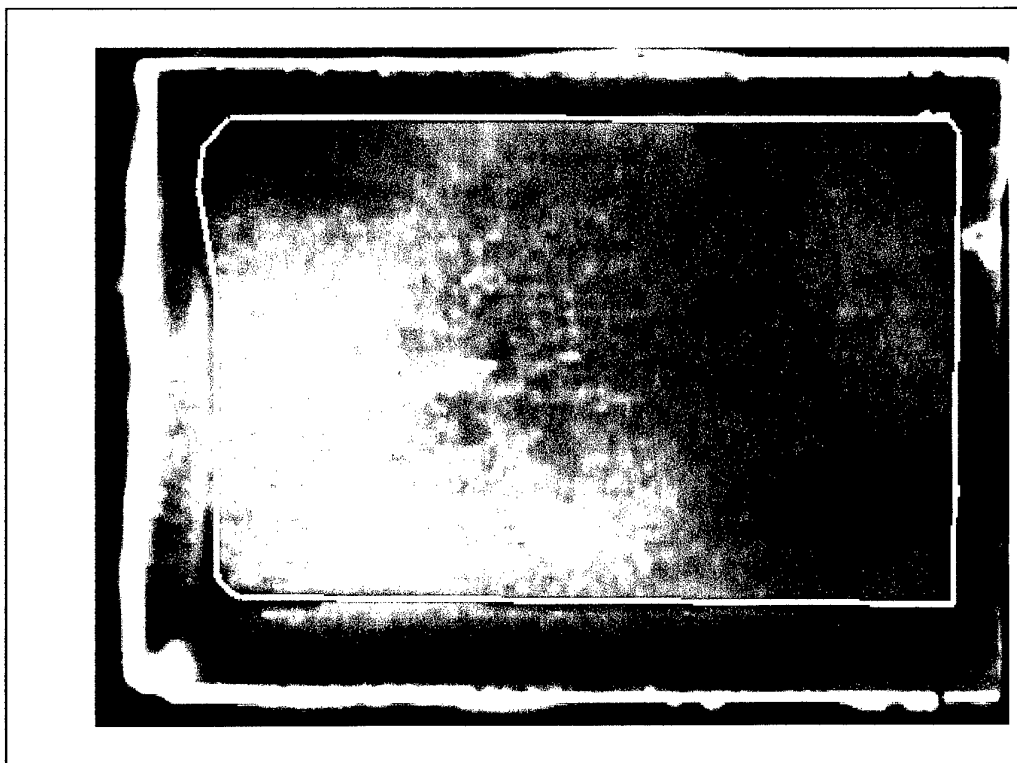
Fig.24
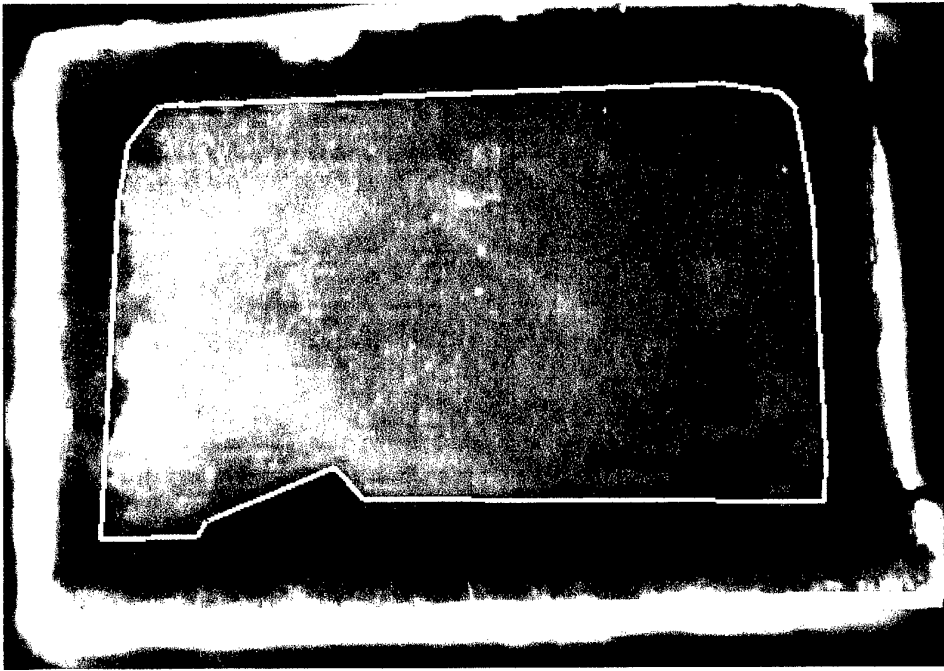
Fig.25
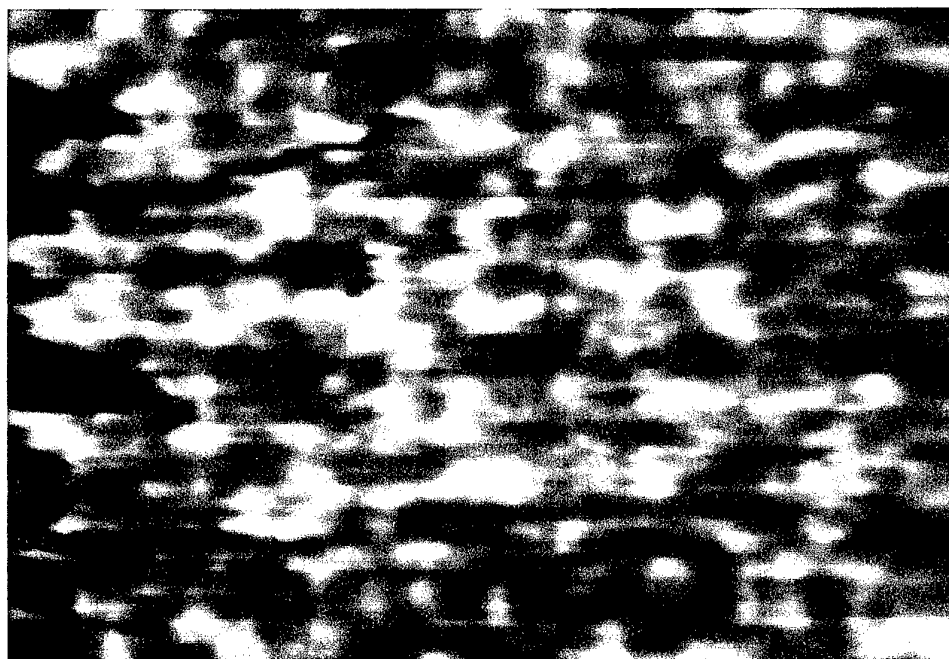
Histograma de R34 a 83.6K

).44   1.00
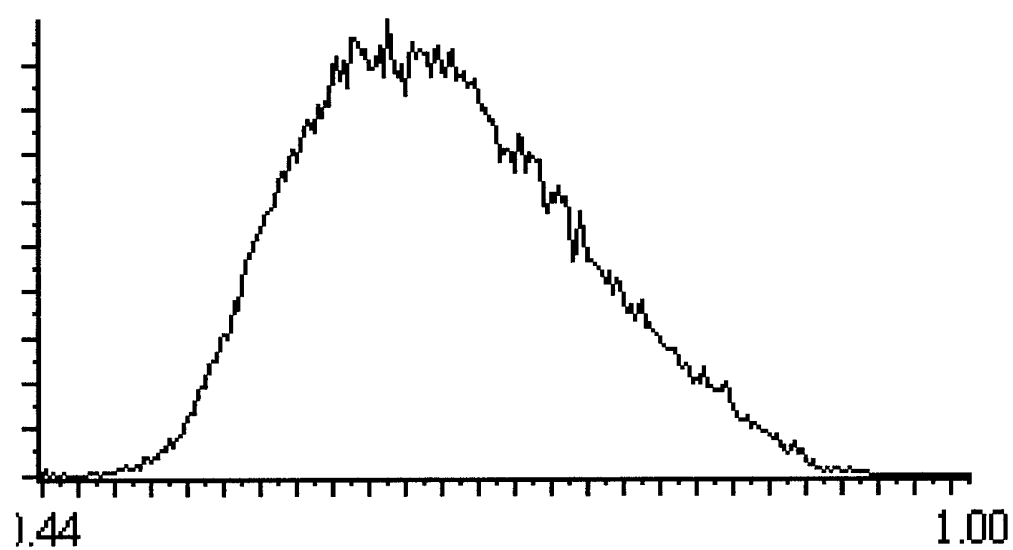
Fig.26
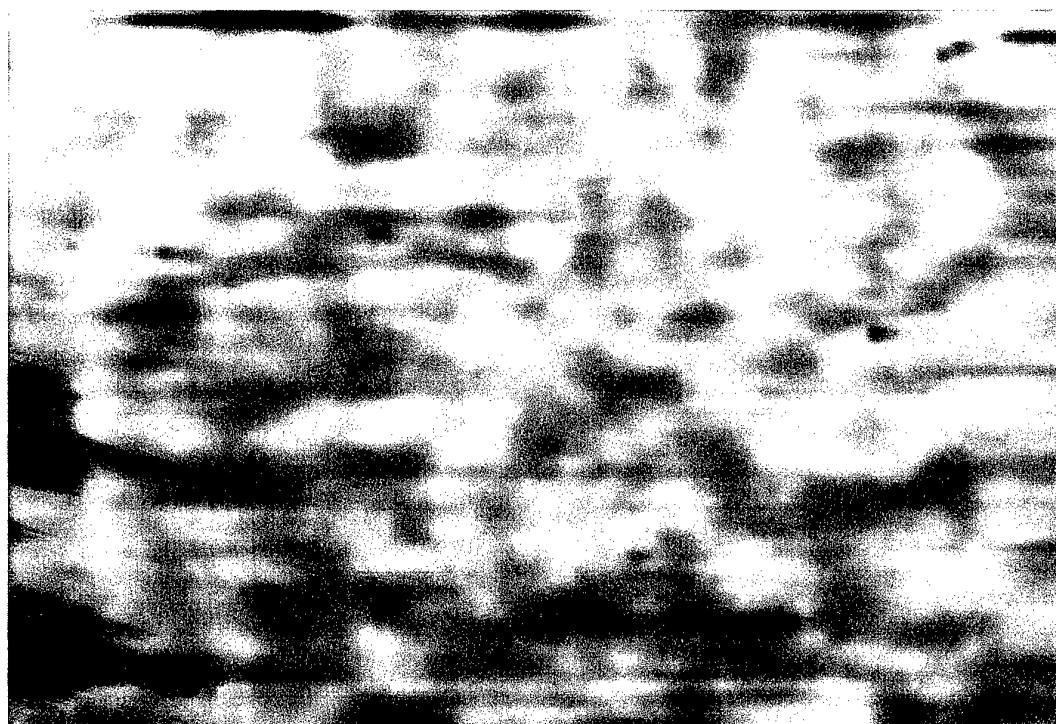
Histograma de R37 a 83.6K

0.78   Luminiscencia   1.00
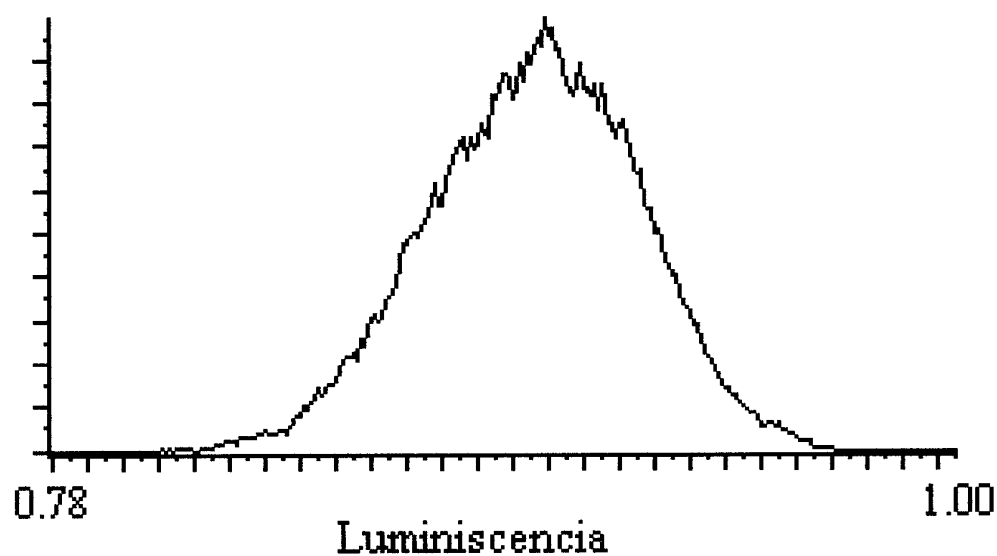
Fig.27
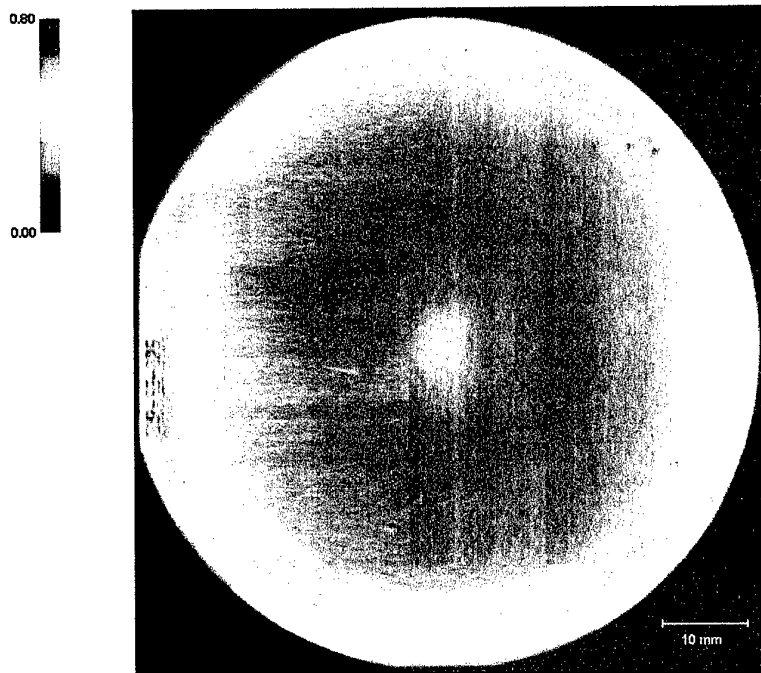
Fig.28
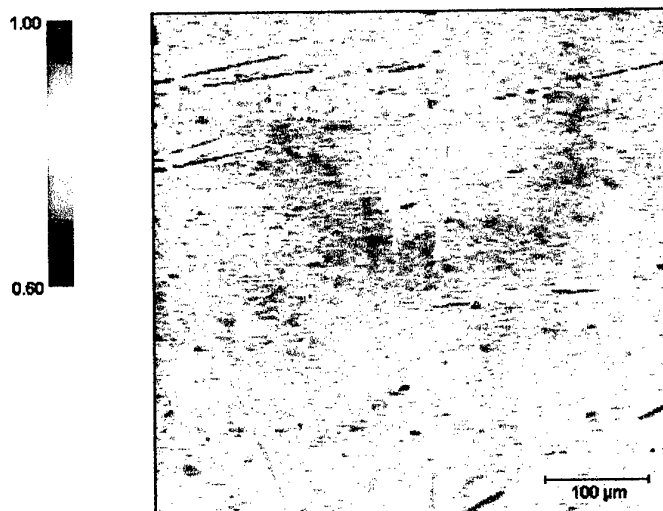
Fig.29
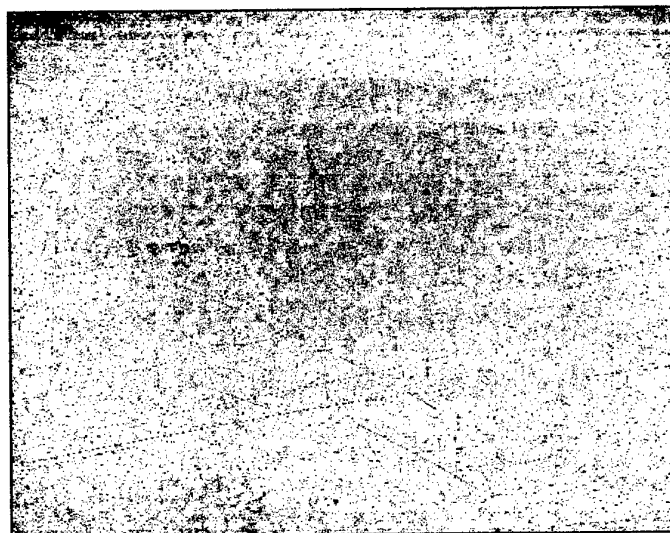
Fig.30

Fig.31

Pin-Ma-55. RE=30, RS=50. X2000 pA. 920 nm

1.800

0.400

50 µm

Fig.32

Fig.33

55-025

Wafer 55 (100)

10^{-5}A

0   59.2 mm

0

24.2 mm

1.04

0.33

InP:Fe W55 (100)
PC Profile

Fig. 34

Wafer 55 (110)

Fig.35

Fig.36

Fig.37

Fig.38